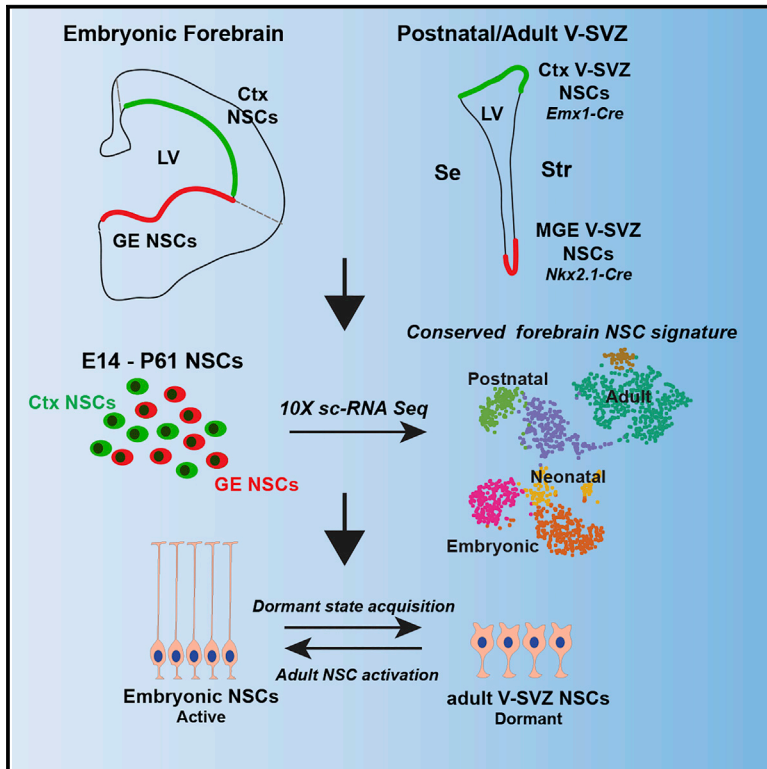


Single-Cell Profiling Shows Murine Forebrain Neural Stem Cells Reacquire a Developmental State when Activated for Adult Neurogenesis

Graphical Abstract



Authors

Michael J. Borrett, Brendan T. Innes, Danielle Jeong, ..., Gary D. Bader, David R. Kaplan, Freda D. Miller

Correspondence

fredam@sickkids.ca

In Brief

Borrett et al. have coupled scRNA-seq with transgenic lineage tracing to define the transcriptional signatures of forebrain mammalian NSCs from embryogenesis to adulthood. They show that dormant adult NSCs share a transcriptional identity with their embryonic parent precursors and reacquire a development-like state when activated to generate adult-born neurons.

Highlights

- Cortex and GE-derived V-SVZ NSCs share a common forebrain NSC signature
- Embryonic NSCs transition to dormant adult NSCs in the first postnatal week
- Adult dormant NSCs acquire a development-like state when reactivated
- Cortex-derived adult NSCs acquire a GE-like state when activated to make neurons



Resource

Single-Cell Profiling Shows Murine Forebrain Neural Stem Cells Reacquire a Developmental State when Activated for Adult Neurogenesis

Michael J. Borrett,^{1,2} Brendan T. Innes,^{3,4} Danielle Jeong,^{1,2} Nareh Tahmasian,^{1,2} Mekayla A. Storer,¹ Gary D. Bader,^{3,4} David R. Kaplan,^{1,2,4} and Freda D. Miller^{1,2,4,5,6,*}

¹Program in Neuroscience and Mental Health, Hospital for Sick Children, Toronto, ON M5G 1L7, Canada

²Institute of Medical Science, University of Toronto, Toronto, ON M5G 1A8, Canada

³The Donnelly Centre, University of Toronto, Toronto, ON M5G 1A8, Canada

⁴Department of Molecular Genetics, University of Toronto, Toronto, ON M5G 1A8, Canada

⁵Department of Physiology, University of Toronto, Toronto, ON M5G 1A8, Canada

⁶Lead Contact

*Correspondence: fredam@sickkids.ca

<https://doi.org/10.1016/j.celrep.2020.108022>

SUMMARY

The transitions from developing to adult quiescent and activated neural stem cells (NSCs) are not well understood. Here, we use single-cell transcriptional profiling and lineage tracing to characterize these transitions in the murine forebrain. We show that the two forebrain NSC parental populations, embryonic cortex and ganglionic eminence radial precursors (RPs), are highly similar even though they make glutamatergic versus gabaergic neurons. Both RP populations progress linearly to transition from a highly active embryonic to a dormant adult stem cell state that still shares many similarities with embryonic RPs. When adult NSCs of either embryonic origin become reactivated to make gabaergic neurons, they acquire a developing ganglionic eminence RP-like identity. Thus, transitions from embryonic RPs to adult NSCs and back to neuronal progenitors do not involve fundamental changes in cell identity, but rather reflect conversions between activated and dormant NSC states that may be determined by the niche environment.

INTRODUCTION

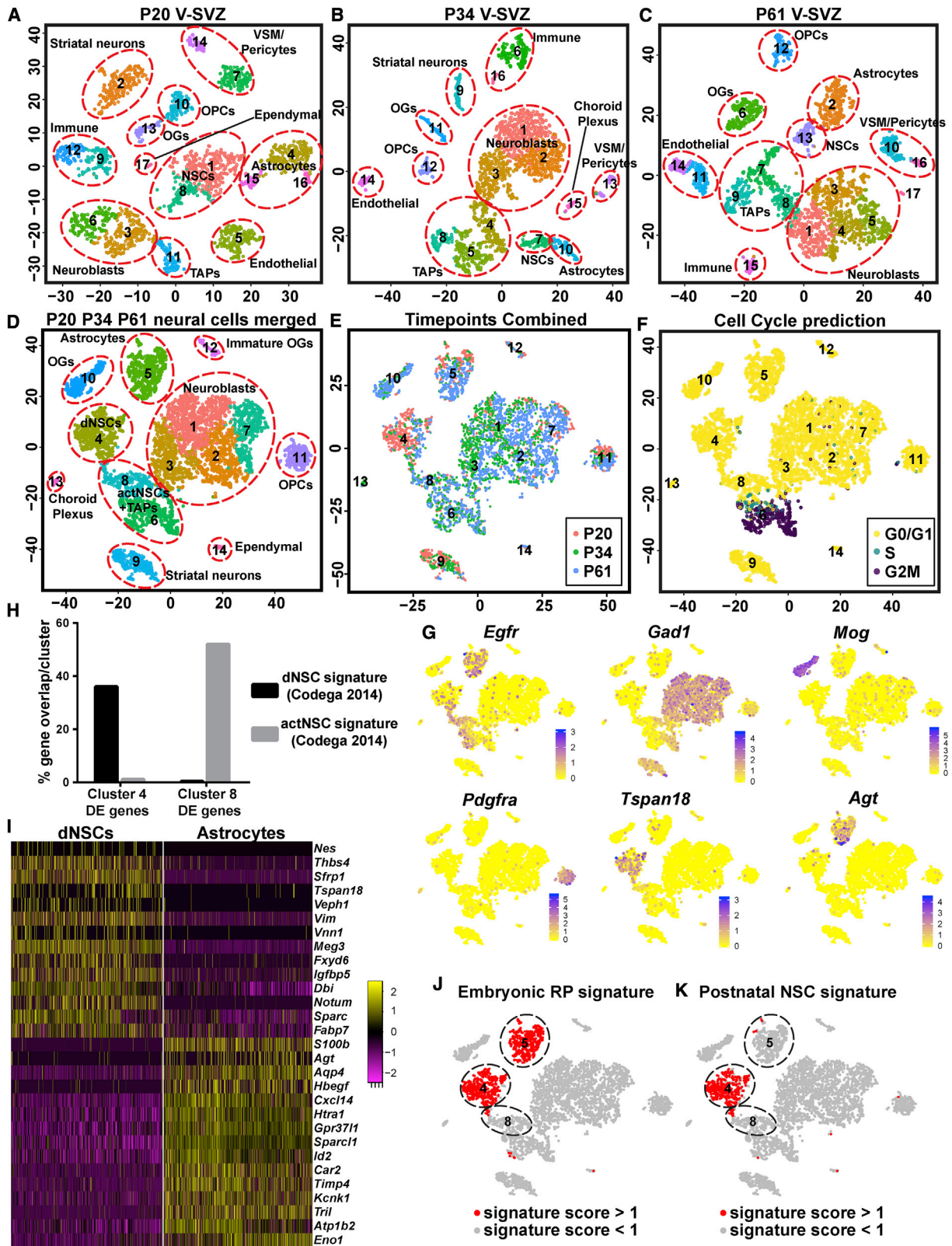
Quiescent adult stem cells are made by embryonic precursors that at the same time build tissues. Different tissues use different strategies to ensure an appropriate establishment of adult stem cell pools. For example, in the gut, the environment induces embryonic epithelial cells to become adult intestinal stem cells (Guin et al., 2019), whereas spermatogonial stem cells instead derive from embryonic precursors that are set aside developmentally (Law et al., 2019). However, we do not yet know how adult neural stem cell (NSC) pools are established in the mammalian brain, although we do know that developmental perturbations can cause long-lasting, functionally important deficits in adult NSCs (for example, see Gallagher et al., 2013, 2015).

One well-studied adult NSC population resides in the forebrain ventricular-subventricular zone (V-SVZ) around the lateral ventricles (Obnier and Alvarez-Buylla, 2019; Miller and Gauthier-Fisher, 2009). These forebrain NSCs derive developmentally from the ganglionic eminence (GE) and cerebral cortex (Merkle et al., 2004; Willaime-Morawek et al., 2006; Young et al., 2007; Kohwi et al., 2007; Ventura and Goldman, 2007; Gallagher et al., 2013), two adjacent embryonic regions containing radial precursors (RPs) that make very distinct progeny. Cortical RPs make glutamatergic excitatory neurons embryonically and

switch at birth to making glial cells, and GE RPs make gabaergic neurons and oligodendrocytes embryonically. Both RP populations then generate V-SVZ NSCs, which make gabaergic interneurons and glial cells postnatally.

Because embryonic cortical RPs and adult V-SVZ NSCs make different types of neurons, this has led to the idea that there is a distinct subpopulation of cortical RPs with gabaergic neuron potential that are fated to become adult NSCs (Morales and Mira, 2019). However, several findings bring this concept into question. First, one definitive lineage tracing study used barcoding to demonstrate that some cortical RPs make excitatory neurons embryonically and gabaergic interneurons postnatally (Fuentelba et al., 2015). Second, single-cell RNA sequencing (scRNA-seq) showed that an embryonic cortical RP gene signature was also expressed by adult V-SVZ NSCs (Yuzwa et al., 2017; Codega et al., 2014), suggesting that these two stem cell populations were more similar than previously appreciated. Third, when embryonic cortical RPs were exposed to a GE environment or cultured as neurospheres, they could make gabaergic interneurons (Hitoshi et al., 2002; Machon et al., 2005; Willaime-Morawek et al., 2006). These findings thus suggest that the same cortical NSCs might be able to make both glutamatergic projection neurons and gabaergic interneurons.





(legend on next page)

Here, we have addressed this possibility by characterizing cortical and GE stem cells throughout life by using scRNA-seq combined with lineage tracing. Our data show that embryonic cortical and GE RPs are highly similar except for a small subset of genes involved in positional information and neuronal specification. As these two RP populations move through developmental time, they transition from a highly active embryonic state to a dormant adult NSC state while maintaining much of their identity. Moreover, when dormant adult NSCs are reactivated to make gabaergic neurons, they reacquire a developing GE RP-like state, regardless of their developmental origin. Thus, our data suggest that embryonic RPs, adult dormant V-SVZ NSCs, and their activated NSC progeny are highly similar stem cells that are in different activation states.

RESULTS

Adult Forebrain NSCs Share Transcriptional Similarities with Embryonic Cortical RPs

To definitively compare embryonic cortical RPs and their adult NSC progeny, we performed scRNA-seq on adult V-SVZ cells. We isolated single cells from dorsal and lateral regions of the V-SVZ at postnatal day 20 (P20), P34, and P61 and used the 10X Genomics platform to sequence 2,182, 2,143, and 2,625 single-cell transcriptomes, respectively (see STAR Methods for details). We analyzed transcriptomes by using a pipeline that incorporates low-level data quality analysis with visualization and clustering methods with evidence-based parameter selection (Innes and Bader, 2019), as described previously (Yuzwa et al., 2017; Carr et al., 2019; Storer et al., 2020). Genes with high variance were used to compute principal components as inputs for projecting cells in two dimensions by using t-distributed stochastic neighbor embedding (t-SNE) and performing clustering using graph-based clustering (Butler et al., 2018) with a range of resolution parameters.

This analysis, together with cell-type-specific marker overlays (see STAR Methods for all markers) identified clusters containing neural and nonneural cells at all 3 time points (Figures 1A–1C; Figure S1A). We removed endothelial cells, microglia, and vasculature-associated mesenchymal cell transcriptomes and combined the remaining neural cell transcriptomes (1,601, 1,847, and 2,185 cells at P20, P34, and P61, respectively). This analysis (Figure 1D) identified 14 clus-

ters, including striatal neurons (9), ependymal cells (14), and choroid plexus cells (13) that were not considered further. The remaining clusters included cells from all time points and were comprised of V-SVZ NSCs and their neurogenic and gliogenic progeny (Figures 1D–1G; Figure S1B). The neurogenic lineage included neuroblasts expressing *Gad1* and *Sp8* (clusters 1, 2, 3, and 7), as well as 2 clusters (6 and 8) of transit amplifying cells (TAPs) and activated NSCs that were both *Egfr* and *Ascl1* positive. Other clusters included *Pdgfra*-positive oligodendrocyte precursor cells (OPCs; 11) and oligodendrocytes (10 and 12).

The 2 remaining clusters, namely, 4 and 5, included cells predicted to be in G1 or G0 that expressed genes shared by NSCs and astrocytes, including *Gfap*, *Glast/Slc1a3*, and *ApoE* (Figures 1D and 1F). Cluster 4 cells fulfilled criteria for slowly proliferating or quiescent adult NSCs; they expressed *Nestin*, *Gfap*, *Vcam1*, *Prom1*, and *Thbs4* and little or no *S100b* and *Agt* (Figure 1G; Figures S1B and S1C). This conclusion was supported by comparing cluster 4 to previously defined sorted V-SVZ NSCs (Codega et al., 2014; Figure 1H; Table S1). Of the genes that were differentially enriched in cluster 4 relative to all other V-SVZ cells (Figure S1D), 36% versus 1.1% were present in gene signatures for sorted quiescent versus activated NSCs. In contrast, genes differentially enriched in cluster 8 activated NSCs/TAPs were found in the sorted activated NSCs. From here on, we term the cluster 4 cells dormant NSCs (dNSCs). Hierarchical clustering showed that these cluster 4 dNSCs were related to but distinct from cluster 5, which instead included astrocytes (Figures 1G and 1I; Figures S1C and S1D). The astrocytes were enriched for *S100b*, *Agt*, *Hbegf*, and *Aqp4*, whereas the dNSCs were instead enriched for genes like *Sfrp1*, *Tspan18*, *Veph1*, *Vimentin*, and *Vnn1*.

We analyzed cluster 4 adult dNSCs for the embryonic cortical RP gene signature that we previously defined (Yuzwa et al., 2017), eliminating genes that were cell cycle associated. All 79 remaining signature genes were expressed in adult dNSCs (Table S2). Most genes (71) were also expressed in astrocytes (Figure S1E), and both dNSCs and astrocytes were highly enriched for a calculated cortical RP gene signature score (Figure 1J; see STAR Methods for details). However, 8 RP signature genes were specific to dNSCs versus astrocytes (*Tfap2c*, *Vim*, *Tead2*, *Sfrp1*, *Rcn1*, *Rcn3*, *Nes*, and *Veph1*) (Table S2), and we combined them with 14 dNSC genes identified by differential gene

Figure 1. Single-Cell Transcriptional Profiling of Murine V-SVZ Cells from P20 to Adulthood

(A–C) t-SNE visualizations of V-SVZ transcriptomes at P20 (A), P34 (B), and P61 (C), annotated for cell types.

(D and E) t-SNEs of combined P20, P34, and P61 V-SVZ neural transcriptomes. Annotated for cell types (D) and color-coded for time point of origin (E). Note that apparent differences in distribution of cells from different time points across clusters were not further analyzed because we performed only a single sequencing run at each time point.

(F) t-SNE showing cell cycle status of dataset in (D) predicted by Cyclone.

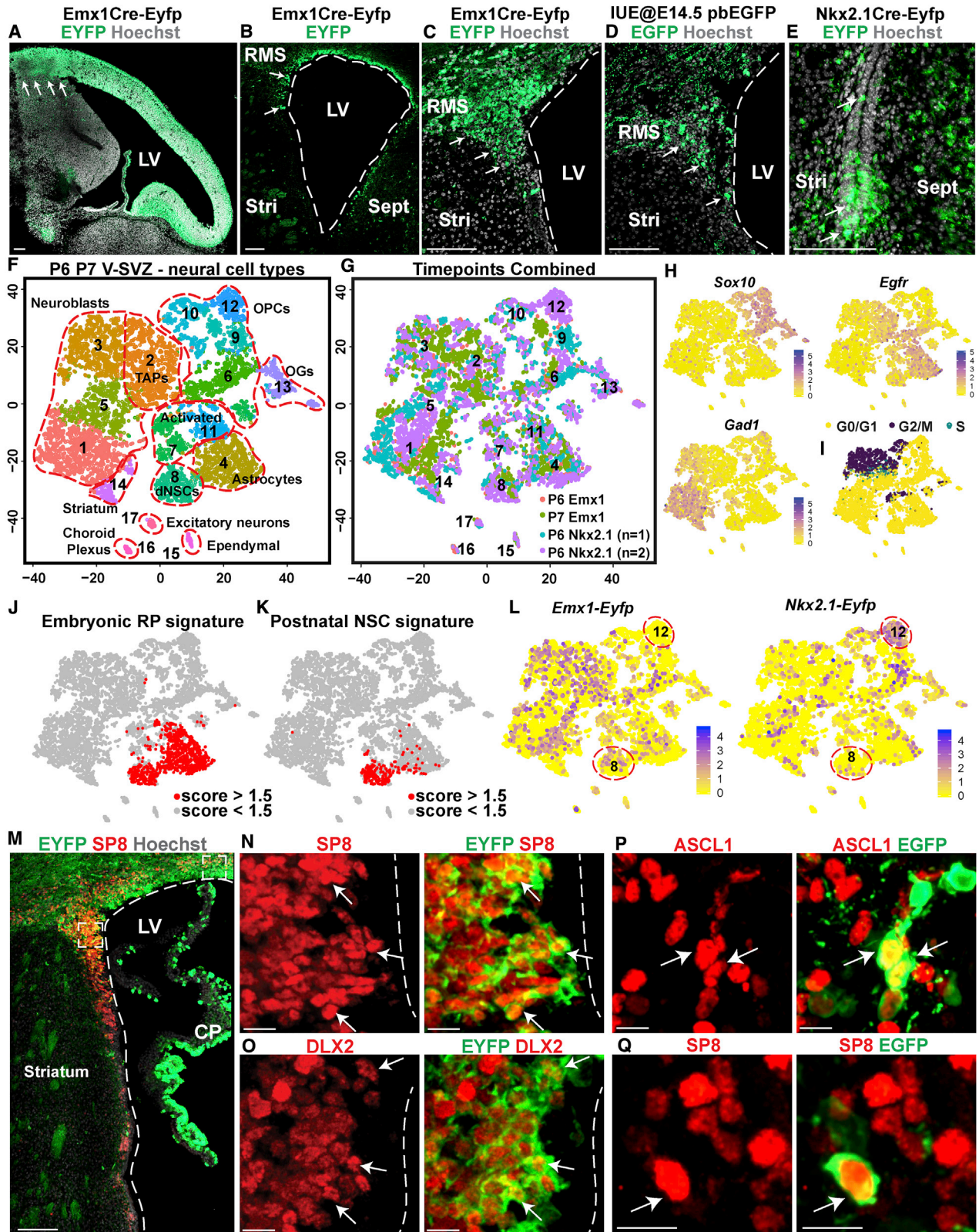
(G) t-SNE marker gene expression overlays of the dataset in (D). Cells are color-coded for levels of expression as per the adjacent color keys.

(H) Percentage of genes differentially enriched (DE) in cluster 4 dNSCs or cluster 8 activated NSCs and TAPs (from D) that were present in gene signatures for sorted quiescent and activated NSCs in Codega et al. (2014). Gene lists are in Table S1.

(I) Heatmap of genes distinguishing dNSCs from astrocytes (clusters 4 and 5 in D). Each column represents expression in a single cell, color-coded as per the adjacent color key.

(J and K) t-SNEs of the dataset in (D) overlaid with signature gene expression scores for embryonic cortical RPs (J) or adult NSCs (K). Red denotes cells with scores of >1 (see STAR Methods).

In (A)–(F), numbers indicate distinct clusters. OGs, oligodendrocytes; VSM, vascular smooth muscle; actNSCs, activated NSCs. See also Figure S1 and Tables S1 and S2.



(legend on next page)

expression analysis (*Thbs4*, *Tspan18*, *Meg3*, *Vnn1*, *Cpe*, *Fxyd6*, *Igf1bp5*, *Dbi*, *Notum*, *Sparc*, *Fabp7*, *Mdfr*, *Shroom3*, and *Ccdc80*) to create a signature that was specific for dNSCs and a small group of activated NSCs in cluster 8 (Figure 1K).

Cortex- and MGE-Derived Cells Contribute to All Neurogenic and Gliogenic V-SVZ Compartments in the First Postnatal Week

We next examined the V-SVZ at P6 and P7 when the dNSC pool is being established. To identify cortically derived cells, we used a well-characterized *Emx1-Cre;R26-LSL-EYFP* transgenic knockin mouse line (called *Emx1Cre-Eyfp* from here on) that tags cortical but not GE cells (Gorski et al., 2002). For comparison, we used a second line that tags cells from the medial GE (MGE) (*Nkx2.1-Cre;R26-LSL-EYFP* or *Nkx2.1Cre-Eyfp* mice) (Xu et al., 2008).

We confirmed the specificity of these mouse lines for lineage tracing. At embryonic day 14 (E14), as predicted (Gorski et al., 2002), the *Emx1Cre-Eyfp* cortex was robustly labeled, with a distinct boundary of EYFP-positive cells at the ventral pallium, a region beside the GE that generates Cajal-Retzius and cortical projection neurons (Dixit et al., 2014; Figure 2A). A few positive cells were found ventral to this boundary, likely migrating precursors or cortical neurons, as previously described (Dixit et al., 2014; Willaime-Morawek et al., 2006; Cocas et al., 2009). Immunostaining and fluorescence *in situ* hybridization (FISH) for the cortical marker *Neurod1* (Figures S2A and S2B) confirmed that *Emx1Cre-EYFP*-positive cells were located at or dorsal to this boundary. We also examined the P6 *Emx1Cre-Eyfp* V-SVZ. For comparison, we used a second lineage tracing approach, electroporating E14.5 cortices with a Piggybac (Pb) transposon-based EGFP reporter (Nagy et al., 2011) that integrates into the genome of cortical RPs and tags all their progeny (Gallagher et al., 2013). At P6, both approaches labeled V-SVZ cells located dorsally and around the dorsolateral corner (Figures 2B–2D; Figure S2C). *Emx1Cre-EYFP* cells were more numerous than *Pb-EGFP* cells, as predicted, but had a similar ventral boundary (Figures 2C and 2D). In contrast, at P6, *Nkx2.1Cre-EYFP*-positive cells were predominantly localized to the ventral-most V-SVZ

(Figure 2E), as previously reported (Delgado and Lim, 2015; Young et al., 2007).

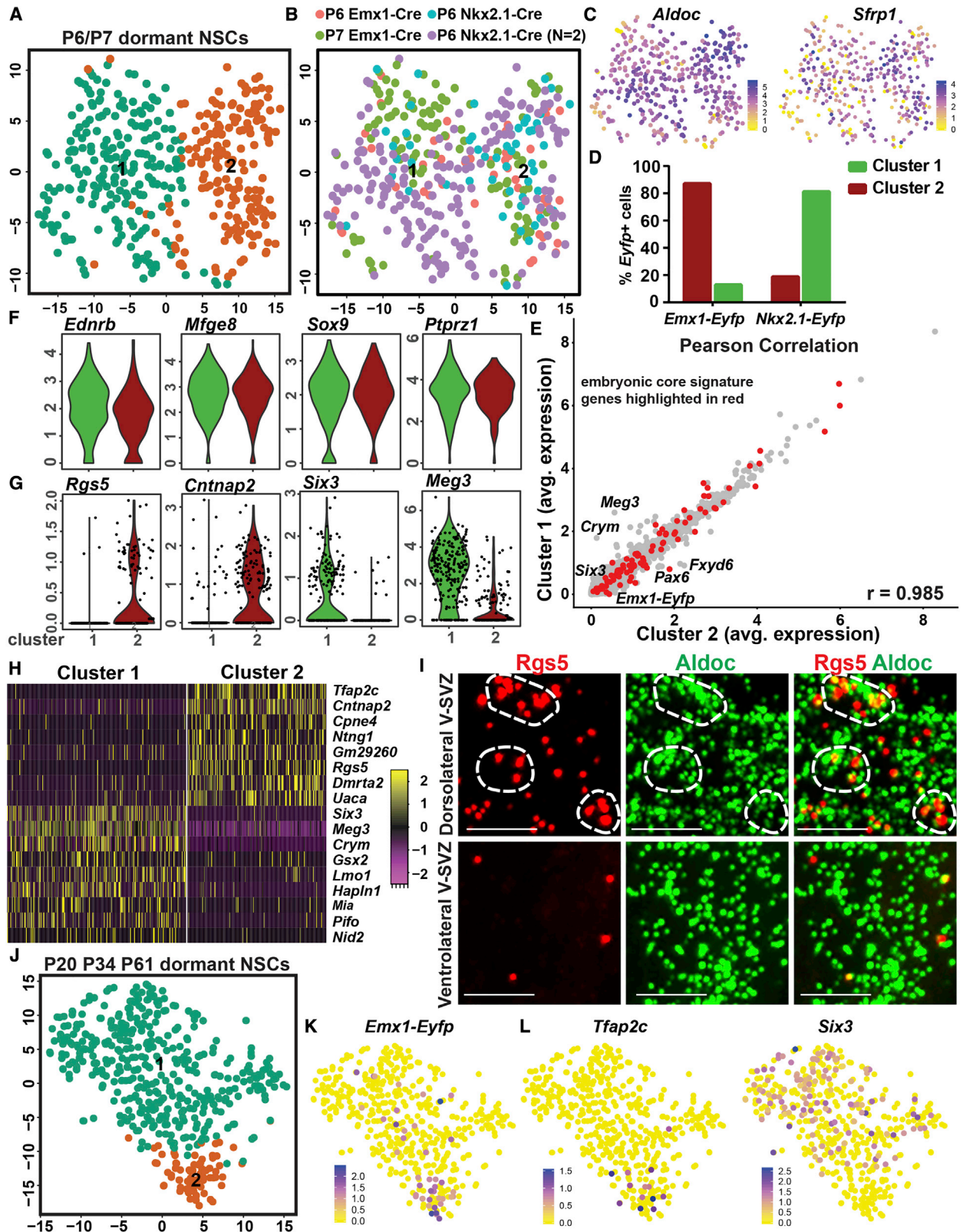
Having validated the lineage tracing, we sequenced 2,725 and 3,431 *Emx1Cre-Eyfp* dorsal and lateral V-SVZ cells at P6 and P7 and 2,234 *Nkx2.1Cre-Eyfp* P6 cells. Because *Nkx2.1Cre-EYFP*-positive V-SVZ NSCs are relatively few (Delgado and Lim, 2015; Figure 2E), we also performed a second run, enriching for *Nkx2.1Cre-EYFP*-positive P6 V-SVZ cells by fluorescence-activated cell sorting (FACS). For all runs, we identified neural and immune cells (Figures S2D and S2E) and then extracted and combined the neural cells alone. This analysis (Figure 2F) identified 17 clusters (7,829 cells), including cells from both mouse lines and all runs with the exception of cluster 12, which included OPCs from only the FACS *Nkx2.1Cre-Eyfp* run. This could be due to a difference in dissection, so we did not analyze this cluster further. We also did not further analyze clusters containing ependymal cells (15), choroid plexus cells (16), striatal neurons (14), or excitatory neurons (17).

The remaining clusters contained dNSCs and their progeny (Figures 2F–2I; Figures S2F and S2G). Four clusters included OPCs (6, 9, and 10) and oligodendrocytes (13). Neuroblasts were in clusters 1, 3, and 5, and proliferative TAPs were in cluster 2. Astrocytes were in cluster 4, and dNSCs were in cluster 8. Both were predicted to be in G0 or G1, and although both clusters were enriched for the embryonic RP gene signature, only cluster 8 dNSCs were enriched for the adult NSC signature (Figures 2J and 2K; Figure S2G; Table S2). The remaining clusters 7 and 11 expressed many NSC and astrocyte genes but also expressed *Egfr* and contained proliferating cells (27% and 16%). We interpret them as activated precursors transitioning from dNSCs to more well-defined gliogenic and neurogenic lineage-biased progenitors. All V-SVZ clusters included both *Emx1-Eyfp*- and *Nkx2.1-Eyfp*-positive cells (Figure 2L). Notably, *Emx1-Eyfp*-positive cells comprised 27% and 40% of the TAPs and neuroblasts, which is indicative of cortical gabaergic neurogenesis.

We confirmed that cortical P6 and P7 NSCs make gabaergic interneurons by immunostaining P6 *Emx1Cre-Eyfp* forebrain V-SVZ sections for DLX2 or SP8 (Figures 2M–2O; Figure S2H).

Figure 2. Lineage Tracing Combined with scRNA-Seq to Characterize Cortex and MGE-Derived P6 and P7 V-SVZ Cells

(A) Stitched sagittal image of the E14 *Emx1Cre-Eyfp* telencephalon, immunostained for EYFP (green). Arrows denote cortex/GE boundary.
 (B) Stitched coronal image of the P6 *Emx1Cre-Eyfp* V-SVZ, immunostained for EYFP (green, arrows).
 (C) Image of P6 *Emx1Cre-Eyfp* V-SVZ, immunostained for EYFP (green). Arrows denote the ventral *Emx1Cre-EYFP*-positive cell boundary.
 (D) Image of a P6 brain electroporated cortically with *Pb-Egfp* at E14.5 and immunostained for EGFP (green), showing a V-SVZ region similar to (C). Arrows denote the ventral *Pb-EGFP*-positive cell boundary.
 (E) Image of the P6 *Nkx2.1Cre-Eyfp* ventral V-SVZ, immunostained for EYFP (green, arrows).
 (F and G) t-SNE of combined *Emx1Cre-Eyfp* and *Nkx2.1Cre-Eyfp* P6/7 V-SVZ neural cells. (F) Is annotated for cell types, and (G) is color-coded for dataset of origin.
 (H) t-SNE marker gene expression overlays of the dataset in (F), color-coded as per adjacent color keys.
 (I) t-SNE showing predicted cell cycle status of dataset in (F).
 (J and K) t-SNEs of dataset in (F) overlaid for signature gene expression scores for embryonic cortical RPs (J) or adult NSCs (K). Red denotes cells with scores of >1.5.
 (L) t-SNEs of the dataset in (F) overlaid for *Emx1-Eyfp* or *Nkx2.1-Eyfp* expression, with cells color-coded as per adjacent color keys.
 (M–O) Images of the P6 *Emx1Cre-Eyfp* dorsolateral V-SVZ immunostained for EYFP (green) and SP8 (red, M and N) or DLX2 (red, O). The lower box in (M) is shown at higher magnification in (N) and the higher box in Figure S2H. Arrows denote double-labeled cells.
 (P and Q) Images of the P4 RMS (P) or P6 dorsolateral V-SVZ (Q) from brains electroporated at E14.5 with *Pb-Egfp*, immunostained for EGFP (green) and ASCL1 (red, P) or SP8 (red, Q). Arrows denote double-positive cells.
 Images in (A), (C)–(E), and (M) show Hoechst 33258 counterstaining (white). In (B)–(D) and (M)–(O), hatched lines outline the lateral ventricle (LV). Stri, striatum; Sept, septum; CP, choroid plexus. Scale bars represent 100 μ m in (A)–(E) and (M) and 10 μ m in (N)–(Q). See also Figure S2 and Table S2.



(legend on next page)

EYFP-positive, DLX2-positive, or SP8-positive cells were found in the dorsal SVZ and in the dorsolateral corner where the rostral migratory stream (RMS) originates. We also immunostained P4 to P7 V-SVZ sections from mice electroporated with the *Pb-Egfp* expression constructs at E14.5 (Figures 2P and 2Q; Figure S2C). Some *Pb-EGFP*-positive cells in the dorsolateral corner were positive for the activated NSC/TAP marker ASCL1 and some for SP8.

Cortex- and GE-Derived dNSCs Are Highly Similar but Maintain Transcriptional Hallmarks of Their Developmental Origins

Cortex-derived NSCs might switch to making gabaergic neurons because they have converged on a GE NSC state. To test this idea, we extracted and reanalyzed the P6 and P7 dNSCs in cluster 8 (Figure 2F). This resulted in two dNSC clusters that included cells from all 4 runs (42% and 38% of *Emx1Cre* cells in clusters 1 and 2, and 58% and 62% of *Nkx2.1Cre* cells in 1 and 2) (Figures 3A–3C). The 2 clusters corresponded to cortex- and GE-derived dNSCs because 87% of cortical *Emx1Cre-Eyfp*-positive cells were in cluster 2 and 81% of *Nkx2.1Cre-Eyfp*-positive cells were in cluster 1 (Figure 3D; Figure S3A). The cortex- and GE-derived dNSC clusters were highly similar, as indicated by correlation analysis ($r = 0.985$) and embryonic RP signature gene expression (Figures 3E and 3F). In contrast, they were relatively dissimilar to their non-proliferative neuroblast progeny ($r = 0.821$; cluster 8 versus 1 and 5 in Figure 2F; Figure S3B). Nonetheless, in spite of their high similarity, cortex and GE dNSCs significantly differentially expressed 119 genes (family wise error rate [FWER] < 0.05 ; Table S3) and some of them were highly enriched in one or the other cluster, including *Tfap2c*, *Rgs5*, and *Dmrt2* in cortex dNSCs and *Six3*, *Lmo1*, and *Gsx2* in GE dNSCs (Figures 3G and 3H; Figure S3A).

We ensured these differences were not due to batch effects by analyzing and obtaining similar results with dNSCs from just the two *Emx1Cre-Eyfp* runs (Figures S2D and S3C–S3E). We also validated one differentially expressed gene by performing FISH for the NSC mRNA *Aldoc* and for *Rgs5* mRNA, which was shown to be enriched in cortex dNSCs (Figure 3I; Figure S3F and S3G). *Aldoc*-positive, *Rgs5*-positive cells were predominantly localized to the dorsolateral corner of the P6 V-SVZ, with no double-positive cells seen more ventrally.

We next asked if cortex- and GE-derived dNSCs were equally similar in adulthood, taking advantage of the fact that the P20, P34, and P61 V-SVZ cells all came from *Emx1Cre-Eyfp* mice. We isolated and analyzed the adult dNSC transcriptomes from cluster 4 (Figure 1D), eliminating any activated NSCs expressing higher levels of *Egfr* and *Ascl1*. Of the 2 resultant clusters, there were 8-fold more *Emx1Cre-Eyfp*-positive cells in cluster 2, and this cluster was also enriched for the P6 and P7 cortical dNSC genes *Tfap2c*, *Cacng5*, *Cpne4*, *Dmrt2*, *Gm29260*, and *Uaca* (Figures 3J–3L). Cluster 1 was instead enriched for the P6 and P7 GE dNSC genes *Crym*, *Six3*, and *Lmo1* (Figure 3L). Nonetheless, these adult cortex and GE dNSCs were highly correlated ($r = 0.976$) (Figure S3H). By contrast, adult dNSCs were poorly correlated with adult neuroblasts ($r = 0.723$; Figure S3I). Thus, cortex and GE dNSCs are highly similar throughout postnatal life but maintain a transcriptional memory of their origins.

Cortical Precursors That Proliferate Late in Embryogenesis Generate Inhibitory Neurons Immediately after Birth

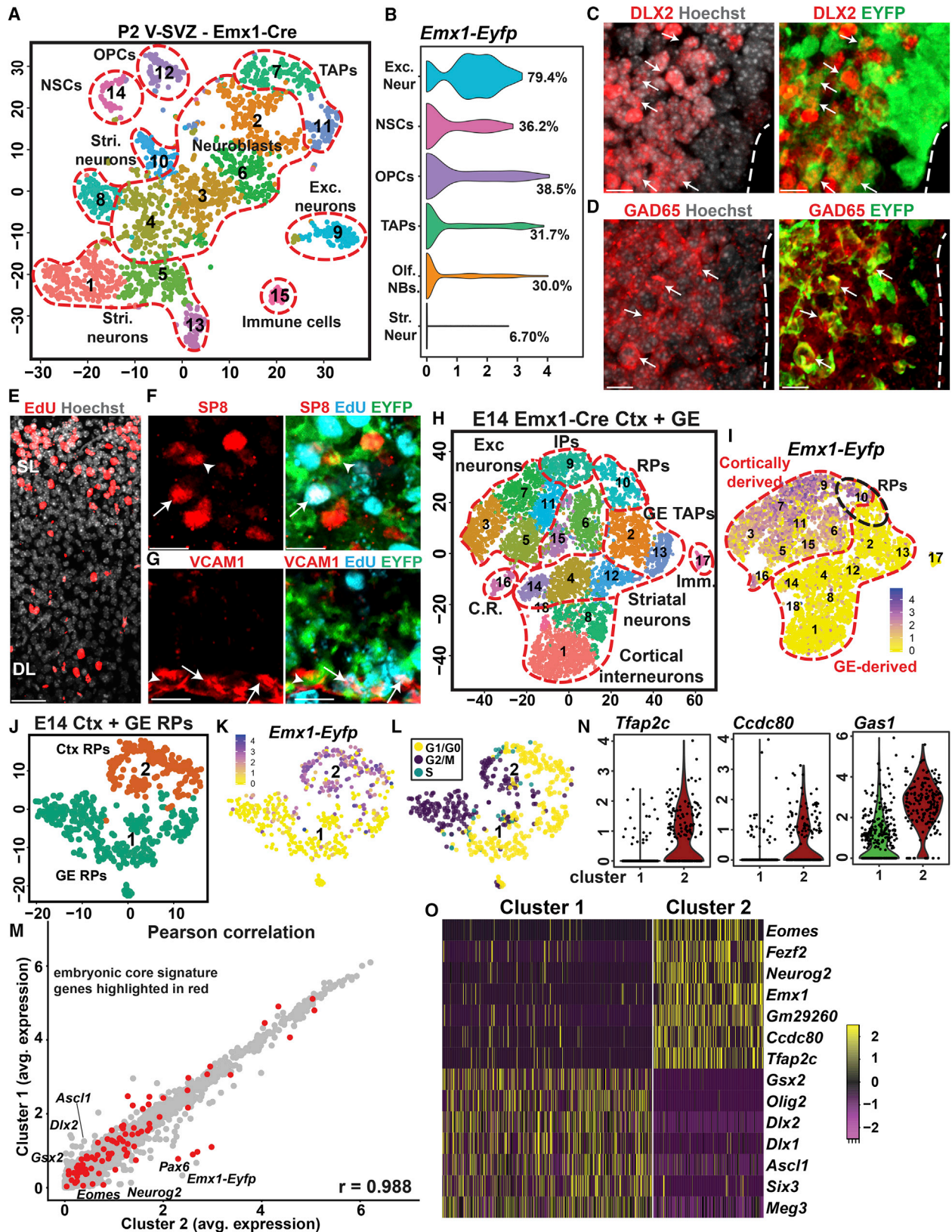
We next asked how early cortex dNSCs make gabaergic interneurons by sequencing 2,252 P2 *Emx1Cre-Eyfp* V-SVZ cells (Figure 4A; Figures S4A and S4B). We identified clusters of V-SVZ neural cells, including OPCs (12), proliferative TAPs (7 and 11), neuroblasts (2, 3, 4, and 6), and NSCs predicted to be in G0 or G1 (14). Astrocytes did not cluster distinctly, likely because they were early in their transition from NSCs. A total of 30%–39% of the NSC, OPC, TAP, and neuroblast clusters were *Emx1Cre-Eyfp* positive (Figure 4B; Figure S4A), indicating that P2 cortical NSCs make gabaergic neuroblasts. We confirmed this finding by immunostaining. At P2, *Emx1Cre-EYFP*-positive cells double-labeled for DLX2, GAD65, or SP8 were present in the dorsal and dorsolateral V-SVZ and the RMS (Figures 4C, 4D, and 4F; Figure S4C).

We asked if the P2 gabaergic neuroblasts were made by cortical RPs proliferating later in embryogenesis; we injected gestational day 16.5 *Emx1Cre-Eyfp* mothers with EdU and analyzed brains of their offspring at P2 (Figure S4D). We observed EdU-positive superficial cortical neurons in these brains, indicating the efficacy of the labeling strategy (Figure 4E). Notably, in 3 independent mice, up to 15% of *Emx1Cre-EYFP*-positive, SP8-positive neuroblasts in the dorsolateral V-SVZ

Figure 3. Postnatal Cortical and GE dNSCs Are Highly Similar but Maintain Transcriptional Hallmarks of Their Developmental Origins

(A and B) t-SNE of combined *Emx1Cre-Eyfp* and *Nkx2.1Cre-Eyfp* P6/7 V-SVZ dNSCs. (A) shows color-coded clusters and (B) is color-coded for dataset of origin. (C) t-SNE marker gene expression overlays of the dataset in (A), color-coded as per adjacent color keys. (D) Percentage of total *Emx1Cre-Eyfp*-positive or *Nkx2.1Cre-Eyfp*-positive dNSC cells in clusters 1 and 2 in (A). (E) Pearson correlation analysis of each detected gene in cluster 2 cortex dNSCs and cluster 1 GE dNSCs in (A). Red denotes embryonic cortical RP signature genes. (F and G) Violin plots of expression profiles for 4 embryonic RP signature genes (F) and 4 differentially-expressed genes (G) in cortical dNSC cluster 2 (maroon) versus GE dNSC cluster 1 (green). Dots in (G) are expression levels in individual cells. (H) Heatmap showing expression of genes that distinguish cortical dNSCs (cluster 2) from GE dNSCs (cluster 1). Each column represents expression in a single cell, color-coded as per the adjacent color key. (I) Images of the P6 dorsolateral (top) and ventrolateral (bottom) V-SVZ probed by FISH for *Rgs5* and *Aldoc* mRNAs (red and green dots, respectively). Dashed lines outline double-labeled cells. Low-magnification images are in Figure S3G. Scale bar represents 10 μ m. (J) t-SNE visualization of combined P20–P61 dNSCs (from Figure 1D) showing color-coded clusters. (K and L) t-SNE gene expression overlays of dataset in (J) showing *Emx1Cre-Eyfp* (K) or two differentially expressed dNSC genes (L), color-coded as per the adjacent color keys.

See also Figure S3 and Table S3.



(legend on next page)

and RMS were also EdU positive, as were some dorsally located EYFP-positive, VCAM1-positive NSCs (Figures 4F and 4G; Figure S4E). Thus, some P2 cortically derived gabaergic neuroblasts are made by RPs that proliferated at E16.5.

Embryonic Cortical and GE RPs Are Also Highly Similar Transcriptionally

To understand the apparent neonatal convergence of cortical and GE NSCs, we sequenced 3 runs of E14 *Emx1Cre-Eyfp* forebrain cells, including the cortex and adjacent GE. We analyzed the runs individually, removed cells with low transcriptome sizes, and combined the datasets. This resulted in 18 clusters (9,909 cells) that contained intermingled cells from all 3 runs (Figure 4H; Figure S4F). *Emx1Cre-Eyfp*-positive and -negative cells clustered separately, with the exception of RP cluster 10 (Figures 4H and 4I; Figure S4G). We did not analyze the *Eyfp*-negative GE clusters in more depth. In addition to RPs, the *Emx1Cre-Eyfp*-positive clusters included intermediate progenitors (9) and excitatory neurons in various maturation stages (3, 5, 7, and 11) (Figure S4H), much as we described for E13.5 (Yuzwa et al., 2017). A total of 80% of cells in these clusters were *Eyfp*-positive, in agreement with the morphological analysis (Figure 2A).

To compare cortex and GE RPs, we analyzed cluster 10 transcriptomes independently (Figures 4J–4L; Figure S4I). One of two resultant clusters (2) was almost entirely comprised of *Emx1Cre-Eyfp*-positive cortical RPs (90%), whereas the other (1) largely contained *Eyfp*-negative GE RPs. These two populations were highly correlated ($r = 0.988$), and 58 cortical RP signature genes were expressed at similar levels in both (Figure 4M). However, some signature genes were highly enriched in cortical cluster 2, including *Tfap2c*, *Ccdc80*, and *Gas1* (Figure 4N; Table S2). A further comparison of cortex and GE RPs identified an additional 118 genes that were significantly differentially expressed with an average expression difference of ≥ 0.5 (FWER < 0.05; Figure 4O; Figure S4J; Table S3). For cortex RPs, they included (1) positional specification genes like *Pax6*, *Emx1*, and *Emx2*; (2) glutamatergic differentiation genes such as *Eomes*, *Fezf2*, and *Neurog2*; and (3) genes enriched in post-

natal cortex NSCs such as *Gm29260*, *Dmrt2a*, *Ccdc80*, and *Tfap2c*. For GE RPs, these genes included (1) gabaergic and oligodendrocyte differentiation genes such as *Gsx2*, *Olig2*, *Olig1*, *Dlx1*, *Dlx2*, and *Ascl1*; and (2) genes enriched in postnatal GE NSCs such as *Six3* and *Meg3*, consistent with a previous GE scRNA-seq analysis (Mayer et al., 2018). Thus, embryonic cortex and GE RPs are highly similar, with the major transcriptional distinction being positional identity and differentiation genes.

Embryonic Cortical RPs Transition to V-SVZ dNSCs between E17 and P6 and P7

To better understand the transition from cortical RPs making excitatory neurons to cortical NSCs making gabaergic neurons, we combined all *Emx1Cre-Eyfp*-positive RPs and NSCs from E14 to P61. We also generated a new dorsal and ventrolateral V-SVZ *Emx1Cre-Eyfp* mouse dataset at E17, when most cortical RPs are slowly proliferating (Fuentelba et al., 2015; Furutachi et al., 2015; Yuzwa et al., 2017). Because RPs are relatively few at E17 (Yuzwa et al., 2017), we flow sorted to enrich for EYFP, sequenced and analyzed the sorted cells to identify *Eyfp*-positive RPs, and then combined them with the other *Eyfp*-positive RPs/NSCs. This analysis (Figures 5A and 5B; Figure S5A) identified 4 clusters, with embryonic and postnatal cells largely segregated. E14 RPs were in 2 clusters, one proliferative (2) and one non-proliferative (1). P6 and P7 dNSCs were in cluster 3 and P20, P34, and P61 dNSCs were in cluster 4. The few E17 RPs were clustered with E14 RPs, and P2 NSCs were scattered between E14 RPs and the P6 and P7 dNSCs.

Trajectory analysis of this dataset using Monocle 2 predicted a linear, single-state trajectory correctly defining the developmental time course (Figure 5C; Figures S5B and S5C). At one end were proliferative and then non-proliferative E14 and E17 RPs. Some E17 RPs extended to meet the P2, P6, and P7 dNSCs, and then they extended to the adult dNSCs at the other end. Glutamatergic differentiation genes like *Neurog2* and *Eomes* as well as cell cycle genes like *Top2a* decreased over this trajectory (Figure 5D; Figure S5D). Thus, cortical precursors transition from RPs to dNSCs from

Figure 4. Analysis of Cortex- and GE-Derived V-SVZ Stem Cells at P2 and E14

- (A) t-SNE of *Emx1Cre-Eyfp* P2 V-SVZ cells, annotated for cell types.
 (B) Violin plots of *Emx1Cre-Eyfp* expression in selected cell types from (A). Also shown are percentages of *Eyfp*-positive cells.
 (C and D) Images of the P2 *Emx1Cre-Eyfp* dorsolateral V-SVZ immunostained for EYFP (green) and DLX2 (red, C) or GAD65 (red, D). Arrows denote double-labeled cells and hatched lines the LVs.
 (E–G) Images of the P2 cortex (E), RMS (F), or dorsal V-SVZ (G) from offspring of *Emx1Cre-Eyfp* mothers injected with EdU on gestational day 16.5 (see schematics in Figure S4D and S4E), analyzed for EdU (red in E, blue in F and G), and immunostained for EYFP (green) plus SP8 (red, F) or VCAM1 (red, G). Arrows denote triple-positive cells, and arrowheads double-positive cells negative for EdU. SL and DL indicate superficial and deep cortical layers.
 (H and I) t-SNEs of E14 *Emx1Cre-Eyfp* cortex and GE cells, annotated for cell types (H) or overlaid for *Eyfp* expression, as per the adjacent color-key (I). Hatched lines distinguish cortical from GE cells. Expression of *Eyfp* in selected clusters is shown in Figure S4G.
 (J and K) t-SNEs of E14 *Emx1Cre-Eyfp* RPs, showing annotated clusters (J) or overlaid for *Eyfp* expression, as per the adjacent color key (K).
 (L) t-SNE showing predicted cell cycle phases for dataset in (J).
 (M) Pearson correlation analysis of each detected gene in GE and cortex RPs in clusters 1 and 2 in (J). Red denotes embryonic cortical RP signature genes.
 (N) Violin plots of expression profiles for 3 differentially expressed genes in cortical RP cluster 2 (maroon) relative to GE RP cluster 1 (green). Dots represent expression levels in individual cells.
 (O) Heatmap showing expression of genes that distinguish cortical versus GE RPs (clusters 2 versus 1). Each column represents expression in a single cell, color-coded as per the adjacent color key.
 Hoechst 33258 counterstaining (white) is shown in (C)–(E). Exc., excitatory; Stri, striatal; Olf. NB, olfactory neuroblasts; C.R., Cajal-Retzius neurons; Imm., immune. Scale bars represent 10 μm in (C), (D), (F), and (G) and 41 μm in (E). See also Figure S4 and Tables S2 and S3.

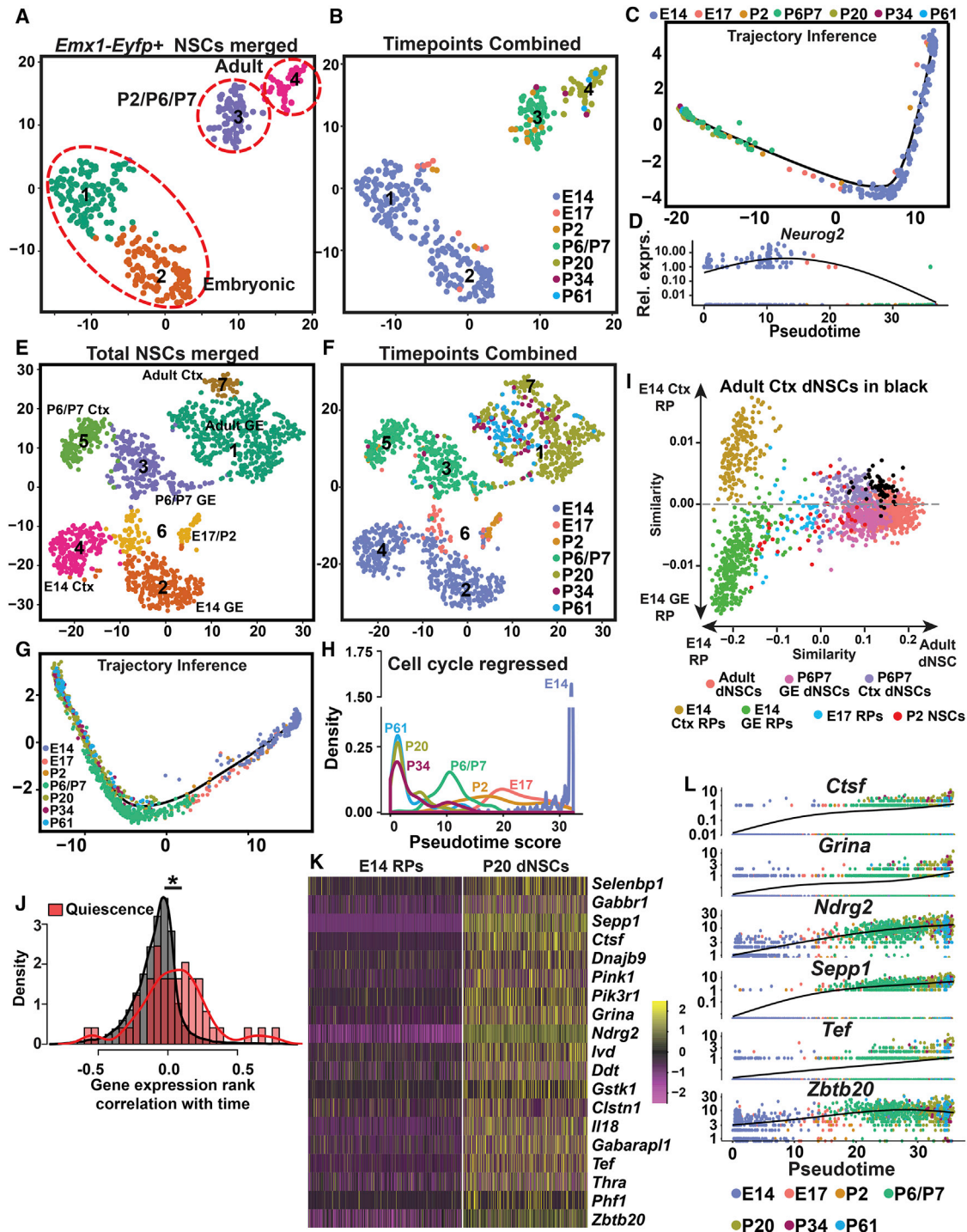


Figure 5. Mapping the Trajectory from E14 RPs to Adult dNSCs with Trajectory and Single-Cell Correlation Analyses

(A) t-SNE of *Emx1-Cre-Eyfp*-positive E14-P61 cortical stem cells, with clusters annotated for developmental age.

(B) t-SNE showing the dataset in (A) with individual cells color-coded to show time point of origin.

(C) Pseudotime ordering of the dataset in (A), determined by Monocle 2 with color-coding to indicate cellular time point of origin. Individual time points are shown in Figure S5C.

(D) Pseudotemporal gene expression dynamics for *Neurog2* in the combined cortical stem cells, with color-coding as in (C), determined by Monocle 2.

(E) t-SNE of total E14-P61 NSC and RPs after cell cycle regression, with clusters annotated for cortex (Ctx) versus GE origin and for developmental time point of origin.

(legend continued on next page)

E17 to P6 and fully acquire an adult dNSC state between P7 and P20.

RPs Transitioning to dNSCs Shut Down Many Cellular Processes while Upregulating Genes Associated with Quiescence and Environmental Sensing

To better define the RP-to-dNSC transition, we increased the power of our analysis by combining cortex and GE RPs and NSCs from E14 to P61 (1,594 cells). To ensure that the cell cycle was not the primary driver of any observed differences, we regressed out cell cycle genes (see STAR Methods). This analysis (Figures 5E and 5F) identified 2 clusters corresponding to each of the E14, P6, P7, and adult NSC datasets. In all cases, one cluster included *Emx1Cre-Eyfp*-positive cortical NSCs and the other *Eyfp*-negative GE NSCs (Figures S6A–S6C). The only exception to this was the E17 and P2 NSCs, which were together in a single cluster (6). We obtained similar results when cell cycle genes were included, except that proliferative versus non-proliferative E14 RPs were segregated into different clusters (Figures S6A–S6C).

We used two approaches to visualize relationships between these NSCs. First, we performed trajectory analysis with the cell cycle-regressed dataset. This defined a single-state linear trajectory that correctly predicted the developmental time course (Figures 5G and 5H; Figure S6D). E14 RPs of both origins were grouped at one end with a few E17 and P2 cells. The other E17 and P2 cells extended to the P6 and P7 dNSCs that extended to and overlapped with the P20, P34, and P61 adult dNSCs. Similar results were obtained when cell cycle genes were included (Figures S6E–S6G). Second, we performed single-cell correlation analysis. As comparators, we determined the average gene expression for E14 cortex versus GE RPs and total E14 RPs versus adult (P20, P34, and P61) dNSCs. We correlated each single-cell transcriptome with these averaged datasets and used this to assign a two-dimensional coordinate for each cell. This analysis (Figure 5I) indicated that (1) P6 and P7 dNSCs are more similar to adult dNSCs than to E14 RPs, (2) E17 and P2 cells are equally similar to E14 and P6 and P7 cells and thus are likely in a transition state, and (3) cortex and GE dNSCs were highly similar at each time point but were not identical.

These two analyses suggest that embryonic RPs undergo a prolonged state change as they transition to dNSCs. We took two approaches to understand this state change. First, we examined a set of quiescence genes identified as upregulated

in adult muscle, hematopoietic, and hair follicle epidermal stem cell microarray datasets (Cheung and Rando, 2013). These quiescence genes were positively correlated over time with the transition from RPs to adult dNSCs, as assessed by gene set enrichment analysis ($p = 0.002$) (Subramanian et al., 2005) and when compared to correlation coefficients of all genes by Wilcoxon rank-sum test (Figure 5J; $p = 1.8e-6$). Of 49 individual genes, 23 were significantly increased ($p < 0.001$) over the RP-to-dNSC transition (Figure S6H), including genes encoding transcriptional regulators such as *Tef*, *Phf1*, *Ezh1*, *Foxo3*, and *Zbtb20* (Figures 5K and 5L).

Second, we performed unbiased global gene set enrichment analysis (GSEA) from E14 to P61. After removing redundant gene sets using a Bayesian network construction approach (Korotkevich et al., 2019), 256 gene sets were significantly decreased over this time frame ($p < 0.01$) (Figure 6A; Table S4). Almost all gene sets involved basic cellular processes required to maintain an active, proliferating stem cell (Figure 6B; Table S4). Conversely, 31 gene sets were significantly enriched in adult dNSCs relative to embryonic RPs, including the quiescence gene set ($p \leq 0.01$; Figure 6A; Table S5). Notably, almost half (48%) were involved in regulating and/or sensing the niche environment, including cues such as nicotine, zinc, neurotransmitters, ions like sodium and potassium, G-protein-coupled receptor ligands, and extracellular matrix proteoglycans.

When Adult NSCs Are Activated to Make Neurons, They Acquire a Developing GE RP-like State

These data suggest that embryonic RPs become adult dNSCs by shutting down their cellular machinery without changing their identity, raising the possibility that when reactivated as adults, they might reacquire an RP-like state. We tested this idea by combining the RP and NSC dataset with activated adult NSCs. We defined activated P20, P34, and P61 NSCs as cells that were positive for the adult NSC gene signature and for *Egfr* and *Ascl1* but were negative for *Dlx2* (cluster 14 in Figure S7A, right panel). We then performed trajectory analysis of this combined dataset with and without cell cycle regression. In both cases (Figures 6C–6F), we obtained single-state trajectories with E14 RPs at one end and adult P20, P34, and P61 NSCs at the other. Notably, in both cases, the distribution of adult activated NSCs was very similar to E17 and P2 transition NSCs.

Because activated adult NSCs were like E17 and P2 transition NSCs, we asked if adult TAPs might be like E14 RPs, performing single-cell correlation analysis as for the combined RP and NSCs

(F) t-SNE showing the dataset in (E) with individual cells color-coded for time point of origin.

(G) Pseudotime ordering of the dataset in (E), determined by Monocle 2 with color-coding to indicate cellular time point of origin.

(H) A density plot of the combined NSC and RP dataset in (G) showing the relative distribution of cells over pseudotime, determined by Monocle 2.

(I) Scatterplot showing differential correlation of single cell transcriptomes with E14 cortex versus GE RP average gene expression (y axis) and with total E14 RP versus adult P20, P34, and P61 dNSC average gene expression (x axis). Individual datasets are color-coded, and cluster 7 adult cortex dNSCs (from E) are highlighted in black. Cell cycle genes were included for this analysis.

(J) Histogram of Spearman rank correlation coefficients of combined E14 to P61 NSCs for the 49 quiescence genes (red) versus all genes (gray). Correlations of > 0 or < 0 indicate expression increases or decreases over time. $*p = 1.8 \times 10^{-6}$, Wilcoxon rank-sum test.

(K) Heatmap showing expression of quiescence genes in E14 RPs versus P20 dNSCs. Each column line represents expression in a single cell, color-coded as per the adjacent color key. Yellow indicates highest expression.

(L) Pseudotemporal gene expression dynamics for 5 quiescence genes in the trajectory analysis of total E14–P61 NSCs that included cell cycle genes (see Figures S6E–S6G), determined with Monocle 2.

See also Figure S5 and S6.

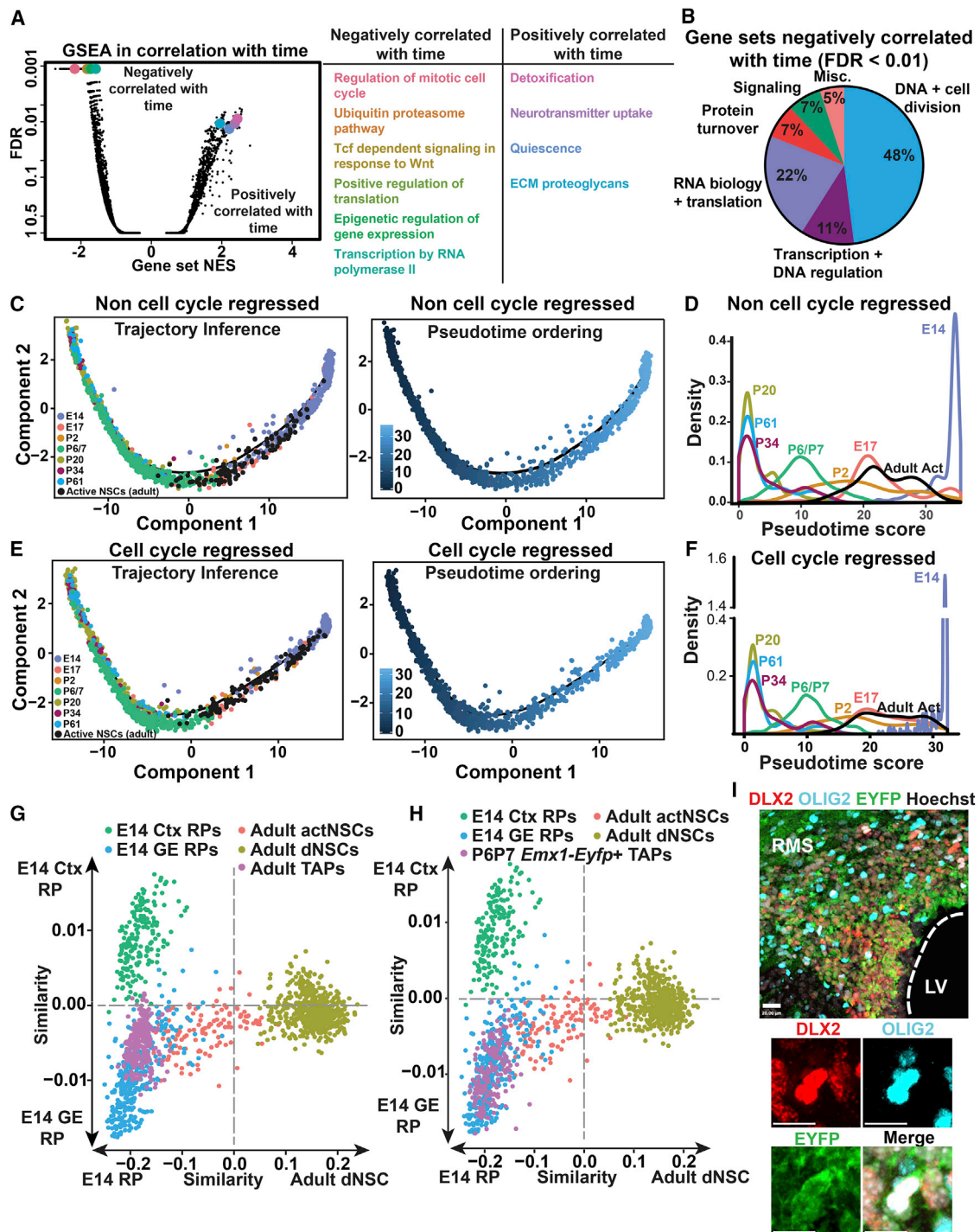


Figure 6. Activated Adult NSCs and TAPs Reacquire a Developing GE RP and NSC-like State

(A and B) GSEA analysis of the combined RP and NSC dataset over time from E14 to P61. (A) A volcano plot showing the gene sets positively and negatively correlated with time. Each dot represents a gene set, and the y axis positions indicate false discovery rate (FDR) (details in Tables S4 and S5). Selected color-coded gene sets are shown to the right. (B) Shows broad categories of gene sets negatively correlated with time (FDR < 0.01). Genes in each category are shown in Table S4.

(C–F) Activated adult NSCs (cluster 14; Figure S7A, right) were combined with the E14–P61 RP and NSCs and the total dataset was analyzed by Monocle 2 without (C and D) and with (E and F) cell cycle regression. (C and E) The resultant trajectory, with cells color-coded for dataset of origin (left) and pseudotime ordering (right). (D and F) Density plots showing the relative distribution of cells from each dataset over pseudotime, with the same color-coding as in (C) and (E).

(legend continued on next page)

(Figure 5I), comparing adult activated NSCs and non-proliferative TAPs to the same averaged datasets. This analysis (Figure 6G; Figures S7B and S7C) indicated that (1) adult activated NSCs were similar to E17 and P2 transition NSCs, (2) non-proliferative adult TAPs were similar to non-proliferative E14 GE RPs, and (3) cortex and GE-derived activated NSCs and TAPs had similar distributions. We obtained similar results when we included P6 and P7 *Emx1Cre-Eyfp*-positive TAPs in the comparison instead of non-proliferative adult TAPs (Figure 6H); cortically derived TAPs were similar to embryonic GE RPs rather than cortical RPs. We validated this similarity *in vivo*, taking advantage of the finding that embryonic GE but not cortical RPs coexpress DLX2 and OLIG2 (Petryniak et al., 2007; Figure S7D). An analysis of P6 *Emx1Cre-Eyfp* forebrain sections showed that in the cortical layers, as predicted, there were EYFP-negative, DLX2-positive interneurons and EYFP-positive, OLIG2-positive OPCs/oligodendrocytes that were DLX2 negative (Figure S7E). However, in the dorsolateral V-SVZ and RMS, we found EYFP-positive cells positive for both DLX2 and OLIG2 (Figure 6I).

Defining Similarities between Adult TAPs and Embryonic GE RPs

To better define similarities between non-proliferative E14 RPs and non-proliferative adult TAPs, we compared both populations to adult dNSCs by using differential gene expression (Figure 7A; Table S6). A total of 87% of genes downregulated in E14 non-proliferative RPs versus adult dNSCs were also downregulated in adult non-proliferative TAPs (FWER < 0.05; ≥ 0.5 log-fold change). Examples of these genes included *Cst3*, *Glu1*, *Atp1a2*, and *Mt1* (Figure 7B). Similarly, 82% of genes enriched in E14 RPs relative to dNSCs were also enriched in TAPs. Examples included *Hmgb3*, *Npm1*, *H2afz*, and *Hnrnpa1* (Figure 7C). Notably, the expression of these genes changed continuously as they transitioned from E14 RPs to adult dNSCs and then back again to activated NSCs and TAPs (Figures 7B and 7C). Consistent with these similarities, non-proliferative E14 RPs and adult TAPs were highly correlated ($r = 0.96$), and only 185 genes were significantly enriched in TAPs and 155 in E14 RPs (FWER < 0.05; ≥ 0.5 log-fold change). Of these 340 DE genes, 104 displayed an expression pattern similar to those seen in Figures 7B and 7C, resulting in 236 distinct DE genes between the two populations (Table S7). Most of these genes differed only in relative expression level but some were highly enriched in one or the other population. For E14 RPs, many of them were NSC-enriched genes such as *Acss1*, *Ddah1*, *Fgfr1*, *Hes1*, *Pdpr*, and *Vit*, whereas for TAPs, they included gabaergic differentiation genes such as *Dlx5*, *Dlx6os1*, *Chga*, *Nptx2*, *Prox1*, and *Gad2* (Figure 7D).

As a second, more global comparison, we performed independent component analysis (ICA), a matrix factorization

approach that allows a definition of components that identify differences in cell state (Saunders et al., 2018). We first performed ICA on the combined RP and NSC dataset to identify components defining differences between dNSCs versus embryonic RPs and E14 cortex versus GE RPs. Optimal separation was achieved with an ICA of 11 components (see STAR Methods), and of these only IC 1 distinguished E14 RPs versus adult dNSCs and IC 11 E14 cortex versus GE RPs (Figure 7E). These two components placed the E17 and P2 NSCs in transition between embryonic RPs and dNSCs, as in our other analyses.

We performed GSEA to identify the genes defining IC 1 and IC 11, including 3 custom gene sets in the analysis; the quiescence-associated gene set (Figure 5J), genes associated with cortical glutamatergic neurogenesis (*Neurog1*, *Neurog2*, *Emx1*, *Emx2*, *Pax6*, *Fezf2*, and *Tbr2*), and a third set associated with GE gabaergic neurogenesis (*Dlx1*, *Dlx2*, *Gsx2*, *Ascl1*, *Olig2* and *Six3*). This analysis showed that almost all gene sets distinguishing E14 RPs from adult dNSCs (ICA 1, x axis) were associated with an active versus dormant cell state (Figure 7F), as seen with the GSEA analysis over time (Figure 6B). The adult dNSCs were instead distinguished by 117 relevant significantly enriched gene sets/pathways, including the quiescence set (false discovery rate [FDR] ≤ 0.01). A total of 27% of these were involved in sensing environmental cues such as ions and neurotransmitters, and 26% were metabolic gene sets with most involved in lipid biology and processing. As predicted, many fewer gene sets/pathways distinguished E14 GE and cortex RPs (ICA 11, y axis) (Figure 7F), with only 15 and 35 pathways enriched in cortical versus GE RPs at a FDR of 5%–10%. For cortical RPs, these pathways included cortex development and glutamatergic differentiation, and for GE RPs, oligodendrocyte/glia differentiation and gabaergic differentiation.

Finally, we projected the normalized and scaled adult activated NSC and non-proliferative TAP transcriptomes into this ICA space (Figure 7G). As for the other analyses, the activated NSCs were located between the adult dNSCs and E14 RPs, and the TAPs were intermingled with the E14 GE RPs. Thus, the transition from an adult dNSC to an activated NSC and ultimately a non-proliferative TAP involves a loss of genes associated with quiescence and the dormant adult NSC state and reacquisition of a developing highly active GE RP-like state that is primed for generation of gabaergic neurons (Figure 7H).

DISCUSSION

A key question is how adult tissue stem cell pools are established developmentally. Here, we present evidence that in the mammalian brain, the transition from an embryonic to an adult NSC does not involve a fundamental change in cell identity but instead reflects a switch from an active to a dormant stem cell state,

(G and H) Scatterplots showing single-cell correlation analysis of E14 GE and cortex (Ctx) RPs, adult dNSCs, and adult activated NSCs (actNSCs) individually correlated with E14 cortex versus GE RP average gene expression (y axis) and with E14 RP versus adult P20, P34, and P61 dNSC average gene expression (x axis). Also included were adult non-proliferative TAPs (G) or P6/7 *Emx1Cre-Eyfp*-positive cortical TAPs (H). Cells are color-coded for dataset of origin. These analyses included cell cycle genes.

(I) Images of the P6 *Emx1Cre-Eyfp* dorsolateral V-SVZ immunostained for EYFP (green), DLX2 (red), and OLIG2 (blue). Bottom images show triple-labeled cells. The hatched line indicates the LV. Scale bar represents 20 μm (top) and 10 μm (bottom images).

See also Figure S7 and Tables S4 and S5.

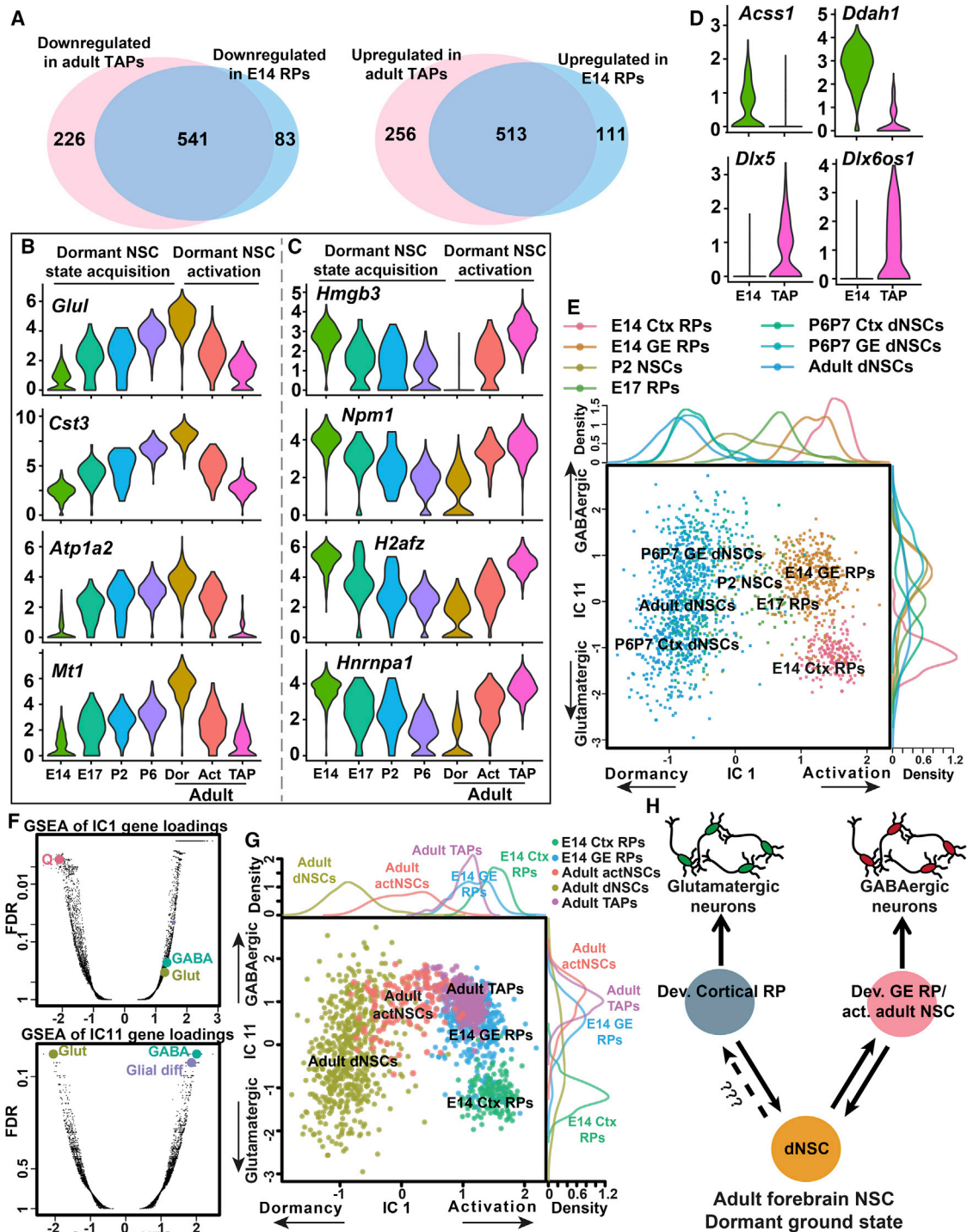


Figure 7. Similarities between Adult TAPs and E14 GE RPs

(A–C) Analysis of differentially expressed genes (FWER < 0.05; ≥ 0.5 log-fold change) in adult dNSCs versus non-proliferative adult TAPs or E14 RPs. (A) Venn diagrams of overlapping genes. (B and C) Violin plots of gene expression profiles over time for selected overlapping genes that were upregulated (B) or downregulated (C) in adult dNSCs.

(D) Violin plots showing expression profiles of selected genes significantly upregulated (top) or downregulated (bottom) in non-proliferative E14 RPs (green) versus adult TAPs (pink).

(E) Scatterplot of ICA analysis, showing the relative position of each individual cell (color-coded for cell type) with regard to IC 1 (x axis) and IC 11 (y axis). Adjacent density plots show the relative distribution of cells from each time point over the x and y axes. Cell cycle genes were included in this analysis.

(legend continued on next page)

potentially as determined by the niche environment (Figure 7H). This model emerged from our analysis of the embryonic RPs that build the striatum and cortex and then ultimately contribute to the adult forebrain dNSC pool. We show that despite their distinct differentiation profiles, cortical and GE RPs are highly similar during embryogenesis and that they maintain this similarity as they transition to an adult dNSC state. When these adult dNSCs are reactivated to make gabaergic neurons, they reacquire a transcriptional state similar to GE RPs, regardless of their developmental origin. We therefore propose that these NSCs share a common ground state/identity and that their niche environment instructs them to proliferate, become quiescent, and/or generate specific types of progeny (Figure 7H).

Our analyses provide a molecular characterization of the NSC transition to and from dormancy. Consistent with other studies of quiescent stem cells (reviewed in van Velthoven and Rando, 2019), including quiescent adult NSCs (Llorens-Bobadilla et al., 2015; Mizrak et al., 2019; Kalamakis et al., 2019; Zywitzka et al., 2018; Basak et al., 2018; Dulken et al., 2017; Shin et al., 2015; Berg et al., 2019; Hochgerner et al., 2018; Artegiani et al., 2017), our data indicate that dormancy involves a broad dampening of cell biological processes associated with an active state. As embryonic RPs transitioned to postnatal dNSCs, they shut down processes associated with cell division, transcription, RNA metabolism and protein translation, processing, and trafficking. However, at the same time adult dNSCs upregulated processes uniquely suited for maintaining them within their niche environment, such as gene sets involving the extracellular matrix and neurotransmitters, consistent with the known importance of these cues for forebrain dNSC biology (Kjell et al., 2020; Obernier and Alvarez-Buylla, 2019).

What cellular mechanisms regulate the developmental transition to dormancy? We did not directly address this question, but we did make two relevant observations. First, we demonstrated upregulation of 23 quiescence genes that are shared with muscle, hematopoietic, and hair follicle epidermal stem cells (Cheung and Rando, 2013). Many of these genes encode transcriptional regulators and receptors and thus may be causally related to quiescence/dormancy. Second, we showed that the transition to dormancy is relatively prolonged. Cortical RPs start to proliferate slowly between E15 and E17, suggesting that this might be when the transition commences (Yuzwa et al., 2017; Fuentealba et al., 2015; Furutachi et al., 2015). However, we show here that E17 RPs and P2 NSCs are still in transition and that a dNSC state is only attained by P6 and P7 with the full adult state achieved at some point between P7 and P20. This protracted

time frame suggests that the quiescence transition might involve several distinct stages. Moreover, the molecular similarity between E17 and P2 transition NSCs and activated adult NSCs and between adult TAPs and GE RPs suggest that reactivation of adult dNSCs might involve a direct reversal of these steps.

Data presented here also address flexibility in NSC differentiation. NSCs are commonly thought to be limited *in vivo* to the genesis of specific classes of neurons, as exemplified by a recent analysis of hippocampal NSCs from embryogenesis through to adulthood (Berg et al., 2019). However, our data suggest that cortex-derived NSCs make excitatory neurons embryonically and inhibitory neurons postnatally and that this is determined by a small subset of flexibly expressed lineage differentiation genes. This model is consistent with several previous findings. First, the loss of a single gene, *Pax6*, caused murine embryonic stem cell (ESC)-derived cortical precursors to make gabaergic rather than excitatory neurons (Nikoletopoulou et al., 2007). Second, when GE RPs were transplanted into an embryonic cortical environment, they made excitatory neurons (Fishell, 1995) and conversely, when cortical RPs were exposed to a GE environment and/or cultured as neurospheres, they made inhibitory neurons (Hitoshi et al., 2002; Machon et al., 2005). Third, during embryogenesis, a small number of cortical RPs migrate into adjacent GE territory, where they appear to acquire a GE RP state (Willaime-Morawek et al., 2006; Cocas et al., 2009).

Together, these findings suggest that the niche environment regulates both the transition between active and dormant forebrain NSCs and the types of daughter cells that are generated, likely by acting upon intrinsic developmentally regulated changes in epigenetic state and/or gene expression repertoire (reviewed in Yao et al., 2016). What then are the relevant environmental cues? As one example, the EGF family (Reynolds et al., 1992; Craig et al., 1996; Codega et al., 2014; Tropepe et al., 1997) and interleukin-6 (IL-6) (Gallagher et al., 2013; Storer et al., 2018) both act to ensure establishment of postnatal forebrain NSC pools by promoting developing NSC proliferation. As a second example, NT-3 (Delgado et al., 2014) and factors deriving from the cerebrospinal fluid (CSF) (Silva-Vargas et al., 2016) regulate the quiescence of adult forebrain NSCs. However, extrinsic factors that promote the developmental transition to quiescence have not yet been identified. Moreover, we still know little about the cues that instruct a cortical NSC to make a glutamatergic versus gabaergic neuron, although a recent paper indicates that *Shh* plays an important role in this decision (Zhang et al., 2020).

(F) IC 1 and IC 11 as analyzed by GSEA. The top volcano plot shows gene sets driving IC 1 that distinguish adult dNSCs from embryonic RPs (negative and positive scores on the x axis indicate upregulated and downregulated in dNSCs, respectively). Each dot represents a gene set, and FDR is indicated on the y axis. The bottom panel shows a similar volcano plot for IC 11, with gene sets that distinguish cortex versus GE RPs (negative and positive enrichment scores on the x axis indicate enriched in cortex versus GE RPs, respectively). Selected gene sets are highlighted. Q, quiescence; GABA, gabaergic differentiation; Glut, glutamatergic differentiation.

(G) Scatterplot showing adult activated NSCs and TAPs projected into the ICA space shown in (E). Axes and density plots are as in (E).

(H) Schematic showing the proposed model, in which highly similar embryonic cortex and GE RPs make excitatory versus inhibitory neurons, respectively. These RPs then transition from a very active stem cell state to a dormant dNSC state between E17 and P6 and attain a fully dormant adult dNSC state by P20. When adult dNSCs of either cortex or GE origin are reactivated, they reacquire a developing NSC state, and their daughter gabaergic neuron-producing TAPs resemble embryonic GE RPs.

See also Tables S6 and S7.

One intriguing prediction of our findings is that adult V-SVZ dNSCs might have the potential to make excitatory projection neurons if reactivated in an appropriate environment. In this regard, Brill et al. (2009) showed that some dorsal V-SVZ NSCs make glutamatergic juxtglomerular neurons for the olfactory bulb and that they may also make cortical neurons after injury, in agreement with a previous report that new cortical neurons are generated after targeted ablation in the adult brain (Magavi et al., 2000). Thus, our findings have important therapeutic implications because they suggest we may be able to unmask an embryonic-like potential in adult NSCs and thus control the types and numbers of progeny they generate if we can ultimately understand the necessary environmental determinants.

STAR★METHODS

Detailed methods are provided in the online version of this paper and include the following:

- KEY RESOURCES TABLE
- RESOURCE AVAILABILITY
 - Lead Contact
 - Materials Availability
 - Data and Code Availability
- EXPERIMENTAL MODEL AND SUBJECT DETAILS
- METHOD DETAILS
 - In utero electroporation
 - Tissue preparation, immunostaining and EdU analysis
 - Antibodies
 - Fluorescence *in situ* hybridization (FISH)
 - Imaging and microscopy
 - Single cell isolation and 10X Genomics sequencing
 - scRNA-seq data analysis pipeline
 - Trajectory inference and pseudotime ordering
 - Cell cycle regression analysis
 - Gene set enrichment analysis
 - ICA data analysis
- QUANTIFICATION AND STATISTICAL ANALYSIS
 - Quantification of gene signature
 - Upregulation of quiescence genes over time
 - Quantification of ambient RNA contamination fraction
 - Differential gene expression statistical analysis
 - Cluster assignment statistical analysis
 - Pearson correlation analysis
 - GSEA statistical analysis
 - Morphological analysis

SUPPLEMENTAL INFORMATION

Supplemental Information can be found online at <https://doi.org/10.1016/j.celrep.2020.108022>.

ACKNOWLEDGMENTS

This work was funded by CIHR and the CFREF “Medicine by Design” to F.D.M., D.R.K., and G.D.B. M.J.B. was funded by CIHR and HSC Restracomp studentships; M.A.S. was funded by OIRM, CIHR, and HSC Restracomp fellowships. We thank Scott Yuzwa, Sarah Burns, Rebecca Parsons, and Dennis Aquino for valuable discussions, technical advice, and assistance; and David Eisenstat for the DLX2 antibody.

AUTHOR CONTRIBUTIONS

M.J.B. conceptualized, performed, and analyzed most of the experiments and co-wrote the paper. B.T.I. performed the GSEA, quiescence gene set, and ICA analyses; D.J. performed and analyzed the P34 and P61 scRNA-seq; N.T. performed FISH and immunostaining; and M.A.S. assisted with the postnatal scRNA-seq. G.D.B. conceptualized and supervised the GSEA and ICA analyses, F.D.M. analyzed data and together with D.R.K. conceptualized experiments and co-wrote the paper.

DECLARATIONS OF INTERESTS

The authors have no conflicts to declare.

Received: March 6, 2020

Revised: May 29, 2020

Accepted: July 21, 2020

Published: August 11, 2020

REFERENCES

- Artegiani, B., Lyubimova, A., Muraro, M., van Es, J.H., van Oudenaarden, A., and Clevers, H. (2017). A single-cell RNA sequencing study reveals cellular and molecular dynamics of the hippocampal neurogenic niche. *Cell Rep.* *21*, 3271–3284.
- Basak, O., Krieger, T.G., Muraro, M.J., Wiebrands, K., Stange, D.E., Frias-Aldieger, J., Rivron, N.C., van de Wetering, M., van Es, J.H., van Oudenaarden, A., et al. (2018). Troy+ brain stem cells cycle through quiescence and regulate their number by sensing niche occupancy. *Proc. Natl. Acad. Sci. USA* *115*, E610–E619.
- Berg, D.A., Su, Y., Jimenez-Cyrus, D., Patel, A., Huang, N., Morizet, D., Lee, S., Shah, R., Ringeling, F.R., Jain, R., et al. (2019). A common embryonic origin of stem cells drives developmental and adult neurogenesis. *Cell* *177*, 654–668.e15.
- Brill, M.S., Ninkovic, J., Winpenny, E., Hodge, R.D., Ozen, I., Yang, R., Lepier, A., Gascón, S., Erdelyi, F., Szabo, G., et al. (2009). Adult generation of glutamatergic olfactory bulb interneurons. *Nat. Neurosci.* *12*, 1524–1533.
- Butler, A., Hoffman, P., Smibert, P., Papalexi, E., and Satija, R. (2018). Integrating single-cell transcriptomic data across different conditions, technologies, and species. *Nat. Biotechnol.* *36*, 411–420.
- Carr, M.J., Toma, J.S., Johnston, A.P.W., Steadman, P.E., Yuzwa, S.A., Mahmud, N., Frankland, P.W., Kaplan, D.R., and Miller, F.D. (2019). Mesenchymal precursor cells in adult nerves contribute to mammalian tissue repair and regeneration. *Cell Stem Cell* *24*, 240–256.e9.
- Cheung, T.H., and Rando, T.A. (2013). Molecular regulation of stem cell quiescence. *Nat. Rev. Mol. Cell Biol.* *14*, 329–340.
- Cocas, L.A., Miyoshi, G., Carney, R.S., Sousa, V.H., Hirata, T., Jones, K.R., Fishell, G., Huntsman, M.M., and Corbin, J.G. (2009). Emx1-lineage progenitors differentially contribute to neural diversity in the striatum and amygdala. *J. Neurosci.* *29*, 15933–15946.
- Codega, P., Silva-Vargas, V., Paul, A., Maldonado-Soto, A.R., Deleo, A.M., Pastrana, E., and Doetsch, F. (2014). Prospective identification and purification of quiescent adult neural stem cells from their *in vivo* niche. *Neuron* *82*, 545–559.
- Craig, C.G., Tropepe, V., Morshead, C.M., Reynolds, B.A., Weiss, S., and van der Kooy, D. (1996). *In vivo* growth factor expansion of endogenous subependymal neural precursor cell populations in the adult mouse brain. *J. Neurosci.* *16*, 2649–2658.
- Delgado, R.N., and Lim, D.A. (2015). Embryonic Nkx2.1-expressing neural precursor cells contribute to the regional heterogeneity of adult V-SVZ neural stem cells. *Dev. Biol.* *407*, 265–274.
- Delgado, A.C., Ferrón, S.R., Vicente, D., Porlan, E., Perez-Villalba, A., Trujillo, C.M., D’Ocón, P., and Fariñas, I. (2014). Endothelial NT-3 delivered by

vasculature and CSF promotes quiescence of subependymal neural stem cells through nitric oxide induction. *Neuron* 83, 572–585.

Dixit, R., Wilkinson, G., Cancino, G.I., Shaker, T., Adnani, L., Li, S., Dennis, D., Kurrasch, D., Chan, J.A., Olson, E.C., et al. (2014). Neurog1 and Neurog2 control two waves of neuronal differentiation in the piriform cortex. *J. Neurosci.* 34, 539–553.

Dulken, B.W., Leeman, D.S., Boutet, S.C., Hebestreit, K., and Brunet, A. (2017). Single cell transcriptomic analysis defines heterogeneity and transcriptional dynamics in the adult neural stem cell lineage. *Cell Rep.* 18, 777–790.

Fishell, G. (1995). Striatal precursors adopt cortical identities in response to local cues. *Development* 121, 803–812.

Fuentealba, L.C., Rompani, S.B., Parraguez, J.I., Oberner, K., Romero, R., Cepko, C.L., and Alvarez-Buylla, A. (2015). Embryonic origin of postnatal neural stem cells. *Cell* 161, 1644–1655.

Furutachi, S., Miya, H., Watanabe, T., Kawai, H., Yamasaki, N., Harada, Y., Imayoshi, I., Nelson, M., Nakayama, K.I., Hirabayashi, Y., and Gotoh, Y. (2015). Slowly dividing neural progenitors are an embryonic origin of adult neural stem cells. *Nat. Neurosci.* 18, 657–665.

Gallagher, D., Norman, A.A., Woodard, C.L., Yang, G., Gauthier-Fisher, A., Fujitani, M., Vessey, J.P., Cancino, G.I., Sachewsky, N., Woltjen, K., et al. (2013). Transient maternal IL-6 mediates long-lasting changes in neural stem cell pools by deregulating an endogenous self-renewal pathway. *Cell Stem Cell* 13, 564–576.

Gallagher, D., Voronova, A., Zander, M.A., Cancino, G.I., Bramall, A., Krause, M.P., Abad, C., Tekin, M., Neilsen, P.M., Callen, D.F., et al. (2015). Ankrd11 is a chromatin regulator involved in autism that is essential for neural development. *Dev. Cell* 32, 31–42.

Gorski, J.A., Talley, T., Qiu, M., Puelles, L., Rubenstein, J.L., and Jones, K.R. (2002). Cortical excitatory neurons and glia, but not GABAergic neurons, are produced in the Emx1-expressing lineage. *J. Neurosci.* 22, 6309–6314.

Guiu, J., Hannezo, E., Yui, S., Demharter, S., Ulyanchenko, S., Maimets, M., Jørgensen, A., Perlman, S., Lundvall, L., Mamsen, L.S., et al. (2019). Tracing the origin of adult intestinal stem cells. *Nature* 570, 107–111.

Helwig, N.E., and Hong, S. (2013). A critique of Tensor Probabilistic Independent Component Analysis: implications and recommendations for multi-subject fMRI data analysis. *J. Neurosci. Methods* 213, 263–273.

Hitoshi, S., Tropepe, V., Ekker, M., and van der Kooy, D. (2002). Neural stem cell lineages are regionally specified, but not committed, within distinct compartments of the developing brain. *Development* 129, 233–244.

Hochgerner, H., Zeisel, A., Lönnerberg, P., and Linnarsson, S. (2018). Conserved properties of dentate gyrus neurogenesis across postnatal development revealed by single-cell RNA sequencing. *Nat. Neurosci.* 21, 290–299.

Innes, B.T., and Bader, G.D. (2019). scClustViz—Single-cell RNAseq cluster assessment and visualization. *F1000Res.* 7, ISCB Comm J-1522.

Kalamakis, G., Brüne, D., Ravichandran, S., Bolz, J., Fan, W., Ziebell, F., Stiehl, T., Catalá-Martinez, F., Kupke, J., Zhao, S., et al. (2019). Quiescence modulates stem cell maintenance and regenerative capacity in the aging brain. *Cell* 176, 1407–1419.e14.

Kjell, J., Fischer-Sternjak, J., Thompson, A.J., Friess, C., Sticco, M.J., Salinas, F., Cox, J., Martinelli, D.C., Ninkovic, J., Franze, K., et al. (2020). Defining the adult neural stem cell niche proteome identifies key regulators of adult neurogenesis. *Cell Stem Cell* 26, 277–293.e8.

Kohwi, M., Petryniak, M.A., Long, J.E., Ekker, M., Obata, K., Yanagawa, Y., Rubenstein, J.L., and Alvarez-Buylla, A. (2007). A subpopulation of olfactory bulb GABAergic interneurons is derived from Emx1- and Dlx5/6-expressing progenitors. *J. Neurosci.* 27, 6878–6891.

Korotkevich, G., Sukhov, V., and Sergushichev, A. (2019). Fast gene set enrichment analysis. *bioRxiv*. <https://doi.org/10.1101/060012>.

Kowalczyk, M.S., Tirosh, I., Heckl, D., Rao, T.N., Dixit, A., Haas, B.J., Schneider, R.K., Wagers, A.J., Ebert, B.L., and Regev, A. (2015). Single-cell RNA-seq reveals changes in cell cycle and differentiation programs upon aging of hematopoietic stem cells. *Genome Res.* 25, 1860–1872.

Law, N.C., Oatley, M.J., and Oatley, J.M. (2019). Developmental kinetics and transcriptome dynamics of stem cell specification in the spermatogenic lineage. *Nat. Commun.* 10, 2787.

Llorens-Bobadilla, E., Zhao, S., Baser, A., Saiz-Castro, G., Zwadlo, K., and Martin-Villalba, A. (2015). Single-cell transcriptomics reveals a population of dormant neural stem cells that become activated upon brain injury. *Cell Stem Cell* 17, 329–340.

Lun, A.T., McCarthy, D.J., and Marioni, J.C. (2016). A step-by-step workflow for low-level analysis of single-cell RNA-Seq data with Bioconductor. *F1000Res.* 5, 2122.

Machon, O., Backman, M., Krauss, S., and Kozmik, Z. (2005). The cellular fate of cortical progenitors is not maintained in neurosphere cultures. *Mol. Cell. Neurosci.* 30, 388–397.

Magavi, S.S., Leavitt, B.R., and Macklis, J.D. (2000). Induction of neurogenesis in the neocortex of adult mice. *Nature* 405, 951–955.

Mayer, C., Hafemeister, C., Bandler, R.C., Machold, R., Batista Brito, R., Jaglin, X., Allaway, K., Butler, A., Fishell, G., and Satija, R. (2018). Developmental diversification of cortical inhibitory interneurons. *Nature* 555, 457–462.

Merkle, F.T., Tramontin, A.D., García-Verdugo, J.M., and Alvarez-Buylla, A. (2004). Radial glia give rise to adult neural stem cells in the subventricular zone. *Proc. Natl. Acad. Sci. USA* 101, 17528–17532.

Miller, F.D., and Gauthier-Fisher, A. (2009). Home at last: neural stem cell niches defined. *Cell Stem Cell* 4, 507–510.

Mizrak, D., Levitin, H.M., Delgado, A.C., Crotet, V., Yuan, J., Chaker, Z., Silva-Vargas, V., Sims, P.A., and Doetsch, F. (2019). Single-cell analysis of regional differences in adult V-SVZ neural stem cell lineages. *Cell Rep.* 26, 394–406.e5.

Morales, A.V., and Mira, H. (2019). Adult neural stem cells: born to last. *Front. Cell Dev. Biol.* 7, 96.

Nagy, K., Sung, H.K., Zhang, P., Laflamme, S., Vincent, P., Agha-Mohammadi, S., Woltjen, K., Monetti, C., Michael, I.P., Smith, L.C., and Nagy, A. (2011). Induced pluripotent stem cell lines derived from equine fibroblasts. *Stem Cell Rev. Rep.* 7, 693–702.

Nikoletopoulou, V., Plachta, N., Allen, N.D., Pinto, L., Götz, M., and Barde, Y.A. (2007). Neurotrophin receptor-mediated death of misspecified neurons generated from embryonic stem cells lacking Pax6. *Cell Stem Cell* 1, 529–540.

Oberner, K., and Alvarez-Buylla, A. (2019). Neural stem cells: origin, heterogeneity and regulation in the adult mammalian brain. *Development* 146, dev156059.

Petryniak, M.A., Potter, G.B., Rowitch, D.H., and Rubenstein, J.L. (2007). Dlx1 and Dlx2 control neuronal versus oligodendroglial cell fate acquisition in the developing forebrain. *Neuron* 55, 417–433.

Qiu, X., Mao, Q., Tang, Y., Wang, L., Chawla, R., Pliner, H.A., and Trapnell, C. (2017). Reversed graph embedding resolves complex single-cell trajectories. *Nat. Methods* 14, 979–982.

Reimand, J., Isserlin, R., Voisin, V., Kucera, M., Tannus-Lopes, C., Rostamianfar, A., Wadi, L., Meyer, M., Wong, J., Xu, C., et al. (2019). Pathway enrichment analysis and visualization of omics data using g:Profiler, GSEA, Cytoscape and EnrichmentMap. *Nat. Protoc.* 14, 482–517.

Reynolds, B.A., Tetzlaff, W., and Weiss, S. (1992). A multipotent EGF-responsive striatal embryonic progenitor cell produces neurons and astrocytes. *J. Neurosci.* 12, 4565–4574.

Saunders, A., Macosko, E.Z., Wysoker, A., Goldman, M., Krienen, F.M., de Rivera, H., Bien, E., Baum, M., Bortolin, L., Wang, S., et al. (2018). Molecular diversity and specialization among the cells of the adult mouse brain. *Cell* 174, 1015–1030.e16.

Scialdone, A., Natarajan, K.N., Saraiva, L.R., Proserpio, V., Teichmann, S.A., Stegle, O., Marioni, J.C., and Buettner, F. (2015). Computational assignment of cell-cycle stage from single-cell transcriptome data. *Methods* 85, 54–61.

Shin, J., Berg, D.A., Zhu, Y., Shin, J.Y., Song, J., Bonaguidi, M.A., Enikolopov, G., Nauen, D.W., Christian, K.M., Ming, G.L., and Song, H. (2015). Single-cell RNA-seq with Waterfall reveals molecular cascades underlying adult neurogenesis. *Cell Stem Cell* 17, 360–372.

- Silva-Vargas, V., Maldonado-Soto, A.R., Mizrak, D., Codega, P., and Doetsch, F. (2016). Age-dependent niche signals from the choroid plexus regulate adult neural stem cells. *Cell Stem Cell* *19*, 643–652.
- Srinivas, S., Watanabe, T., Lin, C.S., William, C.M., Tanabe, Y., Jessell, T.M., and Costantini, F. (2001). Cre reporter strains produced by targeted insertion of EYFP and ECFP into the ROSA26 locus. *BMC Dev. Biol.* *1*, 4.
- Storer, M.A., Gallagher, D., Fatt, M.P., Simonetta, J.V., Kaplan, D.R., and Miller, F.D. (2018). Interleukin-6 regulates adult neural stem cell numbers during normal and abnormal post-natal development. *Stem Cell Reports* *10*, 1464–1480.
- Storer, M.A., Mahmud, N., Karamboulas, K., Borrett, M.J., Yuzwa, S.A., Gont, A., Androschuk, A., Sefton, M.V., Kaplan, D.R., and Miller, F.D. (2020). Acquisition of a unique mesenchymal precursor-like blastema state underlies successful adult mammalian digit tip regeneration. *Dev. Cell* *52*, 509–524.e9.
- Stuart, T., Butler, A., Hoffman, P., Hafemeister, C., Papalexi, E., Mauck, W.M., III, Hao, Y., Stoeckius, M., Smibert, P., and Satija, R. (2019). Comprehensive integration of single-cell data. *Cell* *177*, 1888–1902.e21.
- Subramanian, A., Tamayo, P., Mootha, V.K., Mukherjee, S., Ebert, B.L., Gillette, M.A., Paulovich, A., Pomeroy, S.L., Golub, T.R., Lander, E.S., and Mesirov, J.P. (2005). Gene set enrichment analysis: a knowledge-based approach for interpreting genome-wide expression profiles. *Proc. Natl. Acad. Sci. USA* *102*, 15545–15550.
- Tirosh, I., Izar, B., Prakadan, S.M., Wadsworth II, M.H., Treacy, D., Trombetta, J., Rodman, C., Lian, C., Murphy, G., Fallahi-Sichani, M., et al. (2016). Dissecting the multicellular ecosystem of metastatic melanoma by single-cell RNA-Seq. *Science* *352*, 189–196.
- Trapnell, C., Cacchiarelli, D., Grimsby, J., Pokharel, P., Li, S., Morse, M., Lennon, N.J., Livak, K.J., Mikkelsen, T.S., and Rinn, J.L. (2014). The dynamics and regulators of cell fate decisions are revealed by pseudotemporal ordering of single cells. *Nat. Biotechnol.* *32*, 381–386.
- Tropepe, V., Craig, C.G., Morshead, C.M., and van der Kooy, D. (1997). Transforming growth factor- α null and senescent mice show decreased neural progenitor cell proliferation in the forebrain subependyma. *J. Neurosci.* *17*, 7850–7859.
- van Velthoven, C.T.J., and Rando, T.A. (2019). Stem cell quiescence: dynamism, restraint, and cellular idling. *Cell Stem Cell* *24*, 213–225.
- Ventura, R.E., and Goldman, J.E. (2007). Dorsal radial glia generate olfactory bulb interneurons in the postnatal murine brain. *J. Neurosci.* *27*, 4297–4302.
- Willaime-Morawek, S., Seaberg, R.M., Batista, C., Labbé, E., Attisano, L., Gorski, J.A., Jones, K.R., Kam, A., Morshead, C.M., and van der Kooy, D. (2006). Embryonic cortical neural stem cells migrate ventrally and persist as postnatal striatal stem cells. *J. Cell Biol.* *175*, 159–168.
- Xu, Q., Tam, M., and Anderson, S.A. (2008). Fate mapping Nkx2.1-lineage cells in the mouse telencephalon. *J. Comp. Neurol.* *506*, 16–29.
- Yao, B., Christian, K.M., He, C., Jin, P., Ming, G.L., and Song, H. (2016). Epigenetic mechanisms in neurogenesis. *Nat. Rev. Neurosci.* *17*, 537–549.
- Young, M.D., and Behjati, S. (2020). SoupX removes ambient RNA contamination from droplet based single-cell RNA sequencing data. *bioRxiv*. <https://doi.org/10.1101/303727>.
- Young, K.M., Fogarty, M., Kessar, N., and Richardson, W.D. (2007). Subventricular zone stem cells are heterogeneous with respect to their embryonic origins and neurogenic fates in the adult olfactory bulb. *J. Neurosci.* *27*, 8286–8296.
- Yuzwa, S.A., Borrett, M.J., Innes, B.T., Voronova, A., Ketela, T., Kaplan, D.R., Bader, G.D., and Miller, F.D. (2017). Developmental emergence of adult neural stem cells as revealed by single cell transcriptional profiling. *Cell Rep.* *21*, 3970–3986.
- Zhang, Y., Liu, G., Guo, T., Liang, X.G., Du, H., Yang, L., Bhaduri, A., Li, X., Xu, Z., Zhang, Z., et al. (2020). Cortical neural stem cell lineage progression is regulated by extrinsic signaling molecule sonic hedgehog. *Cell Rep.* *30*, 4490–4504.e4.
- Zywitzka, V., Misios, A., Bunatyan, L., Willnow, T.E., and Rajewsky, N. (2018). Single-cell transcriptomics characterizes cell types in the subventricular zone and uncovers molecular defects impairing adult neurogenesis. *Cell Rep.* *25*, 2457–2469.e8.

STAR★METHODS

KEY RESOURCES TABLE

REAGENT or RESOURCE	SOURCE	IDENTIFIER
Antibodies		
Chicken polyclonal anti-GFP	Abcam	Cat# ab13970; RRID: AB_300798
Rabbit polyclonal anti-SP8	Novus Biologicals	NBP2-49109
Rabbit polyclonal anti-DLX2	Kind gift from Dr. David Eisenstat	N/A
Mouse monoclonal anti-ASCL1	BD PharMingen	Cat# 556604; RRID: AB_396479
Goat polyclonal anti-NEUROD	Santa Cruz	Cat# sc-1084; RRID: AB_630922
Mouse monoclonal anti-GAD65	Abcam	Cat# ab26113; RRID: AB_448989
Rat monoclonal anti-VCAM1	EMD Millipore	Cat# cbl1300; RRID: AB_2214062
Goat polyclonal anti-OLIG2	R & D Systems	Cat# AF2418; RRID: AB_2157554
Biotinylated rabbit polyclonal anti-MBP	Novus Biologicals	Cat# NB110-79873B
Biotinylated monoclonal anti-CD45 antibody	Invitrogen	Cat# 13-0451082
Bacterial and Virus Strains		
NEB 5-alpha Competent <i>E. coli</i> (High Efficiency)	NEB	Cat# C2987H
Biological Samples		
Embryonic, postnatal, and adult SVZ tissue and brains from CD1 and transgenic mice described in Experimental models: Organisms and Strains below.	This paper	N/A
Chemicals, Peptides, and Recombinant Proteins		
5-Ethynyl-2'-deoxyuridine	Invitrogen	Cat# E10187
Propidium Iodide	Abcam	Cat# ab14083
Critical Commercial Assays		
Click-it Edu Cell Proliferation Kit for Imaging, Alexa Fluor 647 dye	Invitrogen	Cat# C10340
RNAscope Fluorescent Multiplex Detection Reagents	ACDBio	Cat# 320851
M.O.M. (Mouse on Mouse) Immunodetection Kit	Vector Laboratories	Cat# BMK-2202
Papain Dissociation System	Worthington	Cat# LK003150
Deposited Data		
scRNA-seq datasets from mouse brains: E14 Cortex + GE Emx1Cre N = 1, E14 Cortex + GE Emx1Cre N = 2, E14 Cortex + GE Emx1Cre N = 3, E17 V-SVZ Emx1Cre, P2 V-SVZ Emx1Cre, P6 V-SVZ Nkx2.1Cre (N = 1), P6 V-SVZ Nkx2.1Cre (N = 2), P6 V-SVZ Emx1Cre, P7 V-SVZ Emx1Cre, P20 V-SVZ Emx1Cre, P34 V-SVZ Emx1Cre, P61 V-SVZ Emx1Cre	This paper	GEO: GSE152281
Experimental Models: Organisms/Strains		
CD1	Charles River	Cat# 022
<i>Emx1Cre/Emx1^{IRRES cre}</i> (B6.129S2- <i>Emx1^{tm1(cre)Krl}/J</i>)	The Jackson Laboratory	Cat# JAX:005628; RRID: IMSR_JAX:005628
<i>Nkx2.1Cre</i> (C57BL/6J-Tg(<i>Nkx2-1-cre</i>)2Sand/J)	The Jackson Laboratory	Cat# JAX:008661 RRID: IMSR_JAX:008661
<i>R26-LSL-Eyfp</i> (B6.129X1-Gt(<i>ROSA</i>)26Sor ^{tm1(EYFP)Cos} /J)	The Jackson Laboratory	Cat# JAX:006148 RRID: IMSR_JAX: 006148)
Recombinant DNA		
<i>PiggyBac</i> eGFP (PCAG-PB-EGFP) and <i>piggybac</i> Transposase plasmids (PCAG-PBase)	Nagy et al., 2011	Nagy et al., 2011
Software and Algorithms		
Adobe Photoshop CC	Adobe Systems	https://www.adobe.com/products/photoshop.html ; RRID:SCR_014199
Adobe Illustrator CC	Adobe Systems	https://www.adobe.com/products/illustrator.html ; RRID:SCR_010279

(Continued on next page)

Continued

REAGENT or RESOURCE	SOURCE	IDENTIFIER
Velocity Image Acquisition Software (Version 6.3)	Perkin Elmer	https://www.perkinelmer.com/lab-solutions/resources/docs/BRO_VelocityBrochure_PerkinElmer.pdf ; RRID:SCR_002668
Zen Image Acquisition Software (Version 2.3)	Zeiss Microscope	https://www.zeiss.com/microscopy/int/products/microscope-software/zen.html ; RRID: SCR_013672
GraphPad Prism 5	GraphPad	https://www.graphpad.com/scientific-software/prism/ ; RRID:SCR_002798
Cell Ranger Software Suite (Versions 2 and 3)	10X Genomics	https://support.10xgenomics.com/single-cell-gene-expression/software/pipelines/latest/installation ; RRID:SCR_016957
R Project for Statistical Computing	R Foundation	https://www.r-project.org/ ; RRID:SCR_001905
Cyclone Cell-Cycle Analysis Algorithm	Scialdone et al., 2015	N/A
Monocle (Version 2)	Qiu et al., 2017 (https://www.nature.com/articles/nmeth.4402)	http://cole-trapnell-lab.github.io/monocle-release/docs/
Seurat R Package (multiple versions)	Stuart et al., 2019 (https://linkinghub.elsevier.com/retrieve/pii/S0092867419305598)	https://satijalab.org/seurat/ ; RRID:SCR_016341
SoupX R Package (Version 0.3.1)	Young and Behjati, 2020 (https://www.biorxiv.org/content/10.1101/303727v2)	https://github.com/constantAmateur/SoupX
fgsea R Package (Version 1.14.0)	Korotkevich et al., 2019 (http://biorxiv.org/lookup/doi/10.1101/060012)	https://bioconductor.org/packages/release/bioc/html/fgsea.html
ica R package (Version 1.0-2)	Helwig and Hong, 2013	https://cran.r-project.org/web/packages/ica/index.html
Other		
FISH probe: Mouse <i>Neurod1</i> (GenBank NM_010894.2) Channel 2	ACDBio	Cat# 416871-C2
FISH probe: Mouse <i>Rgs5</i> (GenBank NM_009063.3) Channel 1	ACDBio	Cat# 430181
FISH probe: Mouse <i>Aldoc</i> (GenBank NM_009657.3) Channel 3	ACDBio	Cat# 429531-C3

RESOURCE AVAILABILITY

Lead Contact

Further information and requests for resources and reagents should be directed to and will be fulfilled by the Lead Contact, Freda Miller (fredam@sickkids.ca).

Materials Availability

This study did not generate new unique reagents.

Data and Code Availability

The scRNA-seq datasets have been deposited in the GEO database under the ID code GEO: GSE152281.

The latest version of the scRNA-seq computational pipeline is available at:

<https://github.com/BaderLab/scRNAseqWorkflow/blob/master/scRNAseqWorkflow.Rmd>

Gene sets defined for GSEA in the study can be found at: http://download.baderlab.org/EM_Genesets/January_01_2020/Mouse_symbol/Mouse_GOBP_AllPathways_no_GO_ia_January_01_2020_symbol.gmt.

The GSEA showing top gene sets associated with components 1 and 11 of the ICA analysis is available at: <https://lab.research.sickkids.ca/miller-kaplan/our-data/>

EXPERIMENTAL MODEL AND SUBJECT DETAILS

All animal use was approved by the Animal Care Committee of the Hospital for Sick Children in accordance with the Canadian Council of Animal Care policies. Mice were fed rodent chow and had free access to water in a 12 hour dark-light cycle room. All mice were well maintained in a healthy state and no mouse displaying any signs of a health or behavioral abnormality was used in the study. For all studies, mice of either sex were used. The age of the mice used in the study ranged from embryonic day 14 (E14) to postnatal day 61 (P61). The specific ages of each animal for each experiment is documented in the results, method details and/or in the figure legends of the study. *Emx1Cre/Emx1^{RES cre}* (B6.129S2-*Emx1^{tm1(cre)Kj}*/J, RRID: IMSR_JAX:005628) (Gorski et al., 2002), *Nkx2.1Cre* (C57BL/6J-Tg(Nkx2-1-cre)2Sand/J, RRID: IMSR_JAX:008661) (Xu et al., 2008), and *R26-LSL-Eyfp* (B6.129X1-Gt(ROSA)26Sor^{tm1(EYFP)Cos}/J, RRID: IMSR_JAX: 006148) (Srinivas et al., 2001) transgenic mouse lines were obtained from Jackson Laboratories. All transgenic mice were in a BL6 background and were bred and genotyped as recommended by Jackson Laboratories. The in utero electroporation experiments, the immunostaining shown in Figure S2A, and the fluorescent *in situ* hybridization shown in Figure 3I were performed with wild-type CD1 mice purchased from Charles River Laboratories.

METHOD DETAILS

In utero electroporation

CD1 timed pregnant mice were purchased from Charles River and were electroporated at E14 as previously described (Gallagher et al., 2013). Briefly, *PiggyBac* EGFP reporter and *PiggyBac* transposase expression constructs (described in Nagy et al., 2011) were co-electroporated at a 1:1 ratio at a concentration of 1 $\mu\text{g}/\mu\text{L}$ per construct (final concentration of 2 μg DNA/ μL). Following injection into the lateral ventricle, the electroporator CUY21 EDIT (TR Tech, Japan) was used to deliver 5 50 ms pulses of 40-50 V with 950 ms intervals per embryo. Brains were harvested postnatally at P4, P6, or P7, as specified, and processed as below.

Tissue preparation, immunostaining and EdU analysis

Brains were dissected from *Emx1-Cre;R26-LSL-EYFP*, *Nkx2.1-Cre;R262-LSL-EYFP*, wild-type or in utero electroporated mice embryonically or in the first postnatal week, fixed in 4% PFA for 24 hours at 4°C, washed in HBSS and transferred to 30% sucrose for 48 hours at 4°C (until brains sank in the sucrose solution). Cryoprotected brains were subsequently embedded in Optimum cutting temperature mounting medium (Tissue-Tek) and stored at -80°C. Frozen embedded brains were sectioned coronally at 16 μm . For immunostaining, brain sections were air-dried at 37°C for 30 min, washed for 5 minutes in 1X PBS and incubated in permeabilization and blocking solution (1X PBS + 5% BSA + 0.3% Triton X-100) for 1 hour at room temperature. Sections were subsequently incubated in primary antibody diluted in 2.5% BSA overnight at 4°C in a humidified chamber. Following primary antibody incubation, sections were washed 3 times in PBS, incubated in secondary antibody (1:1000 dilution in PBS, Invitrogen) for 1 hour at room temperature, washed 3 times in PBS and subsequently counterstained with 0.5 $\mu\text{g}/\text{mL}$ Hoechst 33258 (Sigma-Aldrich) for 5 minutes at room temperature. Slides were then washed and mounted using PermaFluor mounting medium (Thermo Scientific). For mouse anti-GAD65 immunostaining, a mouse on mouse (MOM) kit (Vector Laboratories) was used following the manufacturer's guidelines. For EdU experiments, pregnant female mice were injected with 175 μL of 20mg/mL EdU intraperitoneally at gestational day 16. Brains of their P2 offspring were cryoprotected, sectioned and processed for immunostaining as above. Sections were then fixed a second time with 4% PFA for 20 minutes at room temperature and washed 3 times with PBS. EdU was detected using the Molecular Probes Click-It EdU reaction kit (Invitrogen) as described by the manufacturer. Sections were washed 3 times with PBS, counterstained with 1 $\mu\text{g}/\text{mL}$ Hoechst 33258 for 30 minutes at room temperature, washed and mounted with PermaFluor.

Antibodies

Primary antibodies used were as follows: chicken anti-GFP (Abcam ab13970, 1:1000), rabbit anti-SP8 (Novus NBP2-49109, 1:50), rabbit anti-DLX2 (generously provided by Dr. David Eisenstat, 1:300), mouse anti-ASCL1 (BD PharMingen 556604, 1:1000), goat anti-NEUROD (Santa Cruz, sc-1084, 1:300), mouse anti-GAD65 (Abcam, ab26113, 1:400), rat anti-VCAM1 (EMD Millipore, cbl1300, 1:500), and goat anti-OLIG2 (R & D Systems, AF2418, 1:300). Fluorescently labeled highly cross-absorbed secondary antibodies were purchased from Invitrogen and Jackson ImmunoResearch and used at a dilution of 1:1000.

Fluorescence in situ hybridization (FISH)

Brain sections were prepared as for immunostaining except with RNase-free conditions. RNA was detected using the RNAscope Multiplex Fluorescent Assay Kit (Advanced Cell Diagnostics). Sections were dried for 10 minutes at 37°C, washed in PBS and washed in 50%, 70% and 100% ethanol sequentially for 5, 5, and 2 \times 5 minutes respectively. Sections were permeabilized using the RNAscope Pretreatment-4 solution (Advanced Cell Diagnostics) for 10 minutes at 37°C. RNA probes were preheated at 40°C for 10 minutes and added to the sections and incubated for 2 hours at 40°C. Probes were used to target *Neurod1* (cat. 416871-C2, NM_010894.2), *Rgs5* (cat. 430181, NM_009063.3) and *Aldoc* (cat. 429531-C3, NM_009657.3) mRNAs. Following probe incubation, sections were washed as recommended by the manufacturer and incubated with RNAscope AMP1 solution for 30 minutes at 40°C, washed, incubated with RNAscope AMP2 solution for 15 minutes at 40°C, washed, incubated with RNAscope AMP3 solution for 30 minutes at 40°C, washed, incubated with RNAscope AMP4 solution for 15 minutes at 40°C, washed, and incubated with

0.5 $\mu\text{g}/\text{mL}$ Hoechst 33258 for 5 minutes at room temperature. Tissue slides were mounted in PermaFluor, and positive staining was identified as red or green punctate dots. The scrambled probe provided with the RNAscope kit was used as a negative control. When FISH was coupled with IHC (as shown in Figure S2B), samples were treated as previously described and following, AMP4 incubation and washing, sections were incubated in blocking solution (1X RNase-free PBS + 5% BSA) for one hour at room temperature and then in primary antibody overnight at 4°C. All subsequent immunostaining steps were conducted as for the other experiments ensuring RNase free conditions were maintained.

Imaging and microscopy

Images of immunostaining or FISH were collected using a Quorum spinning disk confocal microscope or a Zeiss Axio Imager M2 microscope with an X-Cite 120 LED light source and a C11440 Hamamatsu camera. For confocal imaging, z stacks were taken, and projected z stacked images are shown.

Single cell isolation and 10X Genomics sequencing

For single cell isolation of the embryonic forebrain, the E14 cortex and GE (predominantly LGE due to the dissection) or regions of the E17 dorsal and lateral V-SVZ were dissected from *Emx1-Cre;R26-LSL-EYFP* mice and cells were mechanically dissociated using a transfer pipette in Neurobasal medium (Invitrogen) supplemented with 2% B27 (Invitrogen), 0.5 mM L-Glutamine (Invitrogen), and 1% Pen-Step (Invitrogen) (neural precursor medium). Following dissociation, cells were filtered through a 70 μm filter and spun down at 1200rpm for 5 minutes. The cell pellet was resuspended in HBSS + 0.25% BSA at a maximum concentration of 5 000 000 cells/mL to which propidium iodide (PI - Abcam) was added at a concentration of 1 $\mu\text{g}/\text{mL}$. The cell suspension was filtered through a 70 μm filter and passed through a Moflo cell sorter (Beckman Coulter) to selectively remove dead/damaged cells (PI-positive). Viable (PI-negative) cells were collected in the neural precursor medium and spun down at 1200rpm for 10 minutes at 4°C. Pelleted cells were resuspended in PBS + 0.04% BSA at a concentration range from 400-700 cells/ μL (cell viability was measured using Trypan blue and was maintained above 80%). Single cell capture and cDNA library preparation was performed at the Princess Margaret Genomics facility (Toronto, ON) or the Hospital for Sick Children Centre for Applied Genomics (Toronto, ON) following the 10X Genomics Chromium system protocol. Single cells were isolated from dorsal and lateral regions of the postnatal V-SVZ at P2, P6 and P7 from *Emx1-Cre;R26-LSL-EYFP* or *Nkx2.1-Cre;R26-LSL-EYFP* brains using essentially the same protocol except that Pasteur pipettes were used for the mechanical tissue dissociation. cDNA library preparation was the same as for the embryonic brain.

For single cell isolation from the P20 *Emx1-Cre;R26-LSL-EYFP* V-SVZ, tissue was incubated in 20 units/mL Papain in 1mM L-cysteine, 0.5mM EDTA and 200 units/mL DNase I (Worthington) dissolved in Hibernate A - minus calcium medium (Brain Bits) for 30 minutes at 37°C. Following enzyme treatment, cells were spun down at 300 g for 5 minutes and resuspended in 2 mL Hibernate A - minus calcium media supplemented with 2% B27. Tissue was triturated using blunt needles with sequentially decreasing diameter (McMaster-Carr). Cells were subsequently spun down at 300 g for 8 minutes and resuspended in Hibernate A - minus calcium medium plus 2% B27. Cells were then filtered through a 70 μm strainer and mixed with superparamagnetic beads (Dynabeads Biotin Binder, Thermofisher 11047) and biotinylated anti-MBP antibody (Novus NB110-79873B) for 30 minutes at 4°C in order to remove myelin from the cell suspension. Following incubation, cells were spun down at 300 g for 8 minutes and resuspended in HBSS plus 0.25% BSA at a concentration of 500 000 cells/mL to which propidium iodide (PI - Abcam) was added at a concentration of 1 $\mu\text{g}/\text{mL}$. Cells were subsequently flow sorted and treated as for the embryonic and neonatal samples. For single cell isolation from the P34 *Emx1-Cre;R26-LSL-EYFP* V-SVZ, the same protocol was followed without the myelin removal step. For single cell isolation from the P61 *Emx1-Cre;R26-LSL-EYFP* V-SVZ, the myelin removal step was not performed, but immune cells were depleted with superparamagnetic beads (Dynabeads Biotin Binder, Thermofisher 11047) and biotinylated anti-CD45 antibody (Invitrogen 13-0451082) after a 30 minute incubation at 4°C. The Papain solution also included the membrane-permeable nuclear dye, DRAQ5 (5mM solution at 3000-fold dilution), allowing for the final collection of PI-negative and DRAQ5-positive viable cells via flow cytometry.

scRNA-seq data analysis pipeline

cDNA libraries were sequenced on an Illumina HiSeq2500 at the Princess Margaret Genomics facility (Toronto, ON) or the Hospital for Sick Children Centre for Applied Genomics (Toronto, ON) at an estimated read depth of 60,000 – 70,000 reads/cell. Sequenced FASTQ reads were processed using Cell Ranger V2 or V3 software (cellranger count function) with settings as recommended by the manufacturer (10X Genomics). Read alignment was performed using a custom reference genome consisting of the *Eyfp* Open Reading Frame concatenated to the Ensembl mm10 reference genome in order to allow for *in silico* detection of the *Eyfp* transgene. Following Cell Ranger data processing, digital gene expression (DGE) matrices were analyzed to determine the average numbers of genes and transcripts (UMIs) detected per cell using genes detected in at least three cells. E14 *Emx1Cre* runs 1, 2 and 3 consisted of an average of 3077, 2754 and 2718 genes/cell and 10221, 9689 and 9672 UMIs/cell, respectively. E17 and P2 *Emx1Cre* runs consisted of an average of 2361 and 2934 genes/cell and 7323 and 9190 UMIs/cell. The P6 and P7 *Emx1Cre* runs consisted of an average of 2611 and 2850 genes/cell and 8753 and 8608 UMIs/cell. P6 *Nkx2.1Cre* runs 1 and 2 consisted of an average of 2560 and 2303 genes/cell and 7466 and 6495 UMIs/cell. P20, P34 and P61 *Emx1Cre* runs consisted of an average of 2012, 2038 and 2003 genes/cell and 5616, 5135 and 4676 UMIs/cell, respectively. DGE matrices were processed through a custom made computational pipeline (previously described in Yuzwa et al., 2017; Carr et al., 2019; Storer et al., 2020; and published in Innes and Bader, 2019).

Briefly, cells with low UMI counts, doublets, contaminant red blood cells and cells with relatively high mitochondrial DNA content were removed. Cell cycle phase of each cell was predicted using the Cyclone method (Scialdone et al., 2015). Genes detected in less than three cells were removed and cell transcriptomes were subsequently normalized as described (Lun et al., 2016) according to their pool and deconvolution normalization method in the *scrn* R package in order to correct for differences in read depth and library size. Normalized expression matrices were imported into Seurat (1.4.0.16) where PCA was performed using highly variable genes in the data. The Seurat function *RunTSNE* was used to generate 2-dimensional t-SNE projections using the top principal components detected in the dataset. The same top principal components were subsequently used to iteratively carry out SNN-Cliq-inspired clustering (*FindClusters* function in Seurat) at increasing resolutions ensuring the number of differentially expressed genes (determined by the *FindMarkers* function in Seurat; $p < 0.01$, family wise error rate [FWER], Holm method) between most similar clusters was greater or equal to 30 genes. In order to account for background gene expression in the datasets due to ambient RNA, which in general ranged from approximately 3% to 7% in datasets from the embryonic and neonatal forebrain, we only analyzed genes that had greater than 5% detection rates in a given cluster.

For the P61 V-SVZ dataset, clusters were assigned at resolution 1.6 (17 clusters identified with at least 50 differentially expressed genes between most similar clusters, FWER < 0.01). For the P34 V-SVZ dataset, clusters were assigned at resolution 1.6 (16 clusters identified with at least 40 differentially expressed genes between most similar clusters, FWER < 0.01). For the P20 V-SVZ dataset, clusters were assigned at resolution 2 (17 clusters identified with at least 160 differentially expressed genes between most similar clusters, FWER < 0.01). To generate the combined P20, P34 and P61 V-SVZ neural dataset, cell barcodes of all neural clusters from each of the three datasets were extracted from the raw DGE matrices and merged prior to running through the pipeline resulting in 5633 cells. Clusters were assigned at a resolution of 0.8 (14 clusters identified with at least 400 differentially expressed genes between most similar clusters, FWER < 0.01). To generate the P20, P34 and P61 V-SVZ dNSC dataset, the combined P20, P34 and P61 V-SVZ neural raw DGE matrix was subsetted to only contain the dNSC barcodes and was subsequently run through the pipeline resulting in 491 cells. Clusters were assigned at a resolution of 0.3 (2 clusters identified with at least 30 differentially expressed genes between most similar clusters, FWER < 0.01). For the P6 *Emx1Cre-Eyfp* V-SVZ dataset, clusters were assigned at resolution 0.8 (11 clusters identified with at least 300 differentially expressed genes between most similar clusters, FWER < 0.01). For the P7 *Emx1Cre-Eyfp* V-SVZ dataset, clusters were assigned at resolution 0.8 (13 clusters identified with at least 150 differentially expressed genes between most similar clusters, FWER < 0.01). For the P6 *Nkx2.1Cre-Eyfp* V-SVZ dataset, clusters were assigned at resolution 0.4 (7 clusters identified with at least 350 differentially expressed genes between most similar clusters, FWER < 0.01). For the P6 *Nkx2.1Cre-Eyfp* V-SVZ dataset (N = 2), clusters were assigned at resolution 0.4 (8 clusters identified with at least 1000 differentially expressed genes between most similar clusters, FWER < 0.01). To generate the combined P6/P7 neural V-SVZ dataset, cell barcodes of all neural clusters from each of the four datasets were extracted from the raw DGE matrices and merged prior to running through the pipeline resulting in 7829 cells. Clusters were assigned at a resolution of 0.8 (17 clusters identified with at least 175 differentially expressed genes between most similar clusters, FWER < 0.01). To generate the P6/P7 V-SVZ dNSC dataset, the combined P6/P7 neural V-SVZ raw DGE matrix was subsetted to only contain the dNSC barcodes and was subsequently run through the pipeline resulting in 390 cells. Clusters were assigned at a resolution of 0.4 (2 clusters identified with 100 differentially expressed genes between most similar clusters, FWER < 0.01). For the P2 V-SVZ dataset, clusters were assigned at resolution of 1.2 (15 clusters identified with at least 85 differentially expressed genes between most similar clusters, FWER < 0.01). For the E17 V-SVZ dataset (data not shown), clusters were assigned at resolution of 1.6 (16 clusters identified with at least 60 differentially expressed genes between most similar clusters, FWER < 0.01). For the E14 forebrain dataset, three independent experiments were performed and all filtered barcodes obtained from each experiment (that had been run through the pipeline) were extracted from the raw DGE matrices and merged prior to being re-run through the pipeline resulting in 9909 cells. Clusters were assigned at a resolution of 1.2 (17 clusters identified with at least 400 differentially expressed genes between most similar clusters, FWER < 0.01). To generate the E14 RP dataset, the combined E14 forebrain raw DGE matrix was subsetted to only contain the RP barcodes and was subsequently run through the pipeline resulting in 523 cells. Clusters were assigned at a resolution of 0.15 (2 clusters identified with at least 210 differentially expressed genes between most similar clusters, FWER < 0.01).

To generate the RP/NSC combined dataset, E14 RPs, E17 RPs, P2 NSCs, P6/P7 dNSCs and combined adult dNSCs were all extracted from their respective raw DGE matrices and merged into one dataset and subsequently run through the pipeline. Cell cycle regression was performed on the same dataset (method described below). Clusters were assigned at a resolution of 0.4 (7 clusters identified with at least 38 differentially expressed genes between most similar clusters, FWER < 0.01). The combined RP/NSC raw DGE was subsetted to only contain the *Emx1Cre-Eyfp*-positive cells (*Emx1-Eyfp* detected expression > 0) in order to generate the *Emx1Cre-Eyfp*-positive RP/NSC combined dataset resulting in 356 cells (shown in Figure 5A). Clusters were assigned at a resolution of 0.8 (4 clusters identified with at least 180 differentially expressed genes between most similar clusters, FWER < 0.01). P20, P34 and P61 activated NSCs were identified by analyzing the combined adult neural dataset at a higher clustering resolution of 1.6 as shown in Figure S7A (18 clusters identified with at least 150 differentially expressed genes between most similar clusters, FWER < 0.01) and were merged to the combined RP/NSC raw DGE and subsequently processed in Monocle 2 (see below). To generate the combined RP/NSC/activated NSC/adult TAP dataset, the activated adult NSCs and non-proliferative adult TAPs (TAPs that were not in S, G2 or M phase as predicted by Cyclone; the TAPs in cluster 8 of Figure 1D) were merged to the combined RP/NSC raw DGE and were subsequently normalized using the aforementioned method in the *Scrn* R package. Differential gene expression analysis for this dataset was performed using the *FindMarkers* function in Seurat v.3.1.1 using an adjusted p value cutoff of 0.05 (Bonferroni correc-

tion). Note that for all dataset merging, the union of all detected genes from each dataset was always used. t-SNE gene overlays were generated using the Seurat FeaturePlot function, violin plots were generated using the Seurat VlnPlot function, heatmaps were generated using the Seurat DoHeatmap function (using scaled expression values) and hierarchical clustering was obtained using a custom designed Shiny Script.

To identify all cell types except NSCs and astrocytes, we used the following well-defined marker genes - for endothelial cells, *Pecam1/Cd31*, *Plvap*, *Esam*; for vasculature-associated mesenchymal cells, *Pdgfrb*, *Myh11*, *Mylk*; for immune cells, *Aif1*, high *Cx3cr1*; for ependymal cells, *Foxj1*, *S100b*; for choroid plexus cells, *Ttr*; for cortical excitatory neurons, *Neurod2*, *Tbr1*, *Satb2*; for OPCs, *Pdgfra*, *Sox10*, *Olig2*; for mature oligodendrocytes, *Sox10*, *Olig1*, *Mbp*, *Mog*, *Mag* but not *Pdgfra*; for immature oligodendrocytes, as for the mature oligodendrocytes but in addition positive for *Enpp6* but not *Mog*; for TAPs, *Egfr*, *Ascl1*, *Dlx1*, *Dlx2* but not *Sp8* or *Gad* genes; for neuroblasts, *Gad1*, *Gad2*, *Dlx1*, *Dlx2*, *Sp8*; for intermediate progenitors, *Eomes*, *Neurod1*, *Gadd45g*, *Sstr1*. For postnatal NSCs and astrocytes, we used the shared well-characterized marker genes *Gfap*, *Glast/Slc1a3*, *ApoE* and *Aldoc*, as well as the shared genes from the embryonic cortical RP gene signature. For astrocytes versus NSCs, we used the previously-characterized markers *S100b* and *Agt* for astrocytes and *Nestin*, *Vimentin*, *Prom1* and *Thbs4* for NSCs. We also used the differentially-expressed genes we identified, presented in Figures 1F–1J. We identified activated NSCs as expressing *Egfr* and *Ascl1* but not *Dlx* genes and being positive for the embryonic RP and NSC-specific gene signatures.

Trajectory inference and pseudotime ordering

Single cell pseudotime trajectories were constructed using a modified version of the dpFeature method in *Monocle v2* (Trapnell et al., 2014) as described (Storer et al., 2020). Briefly, cell barcodes from desired datasets were extracted from the raw digital gene expression matrices and merged prior to normalization using Monocle’s size factor normalization method. PCA was performed using the same highly variable genes that were obtained from our custom built pipeline as described above and the cells were projected into 2-dimensional space using the tSNE algorithm. Cells were subsequently assigned into distinct clusters using Monocle’s density peak clustering algorithm. A set of ordering genes was obtained by testing each gene for differential expression between the clusters in the dataset and selecting the top 1000 significantly differentially expressed genes. Expression profiles were reduced to 2 dimensions using the DDRTree algorithm included in Monocle 2 and cells were ordered using these genes to obtain a trajectory. Gene expression was plotted over pseudotime using Monocle’s `plot_genes_in_pseudotime` function in which the `sm.ns` function in the *VGAM* package was used to model gene expression over pseudotime as a continuous non-linear function. In some cases, cell cycle regression was performed as described below.

Cell cycle regression analysis

Cell cycle regression was carried out by removing all cell cycle related genes from the highly variable genes used to perform PCA. All downstream steps were performed as previously described. In order to carry out cell cycle regression on the trajectory inference analysis performed using Monocle, the same list of cell cycle related genes were removed from the top 1000 differentially expressed genes used to order the cells along the inferred trajectory. In order to obtain a list of cell cycle related genes, we took the enriched genes from all G1, S, and G2/M marker gene pairs used by the Cyclone method to assign cell cycle phase that were detected in our single cell RNA-Seq dataset. These genes were subsequently combined with an additional list of S phase related and G2/M phase related genes described in Kowalczyk et al. (2015) and Tirosh et al., 2016 (same cell cycle genes that are used to assign cell cycle scores in Seurat v3). Together this resulted in a total of 678 cell cycle related genes that were used to perform cell cycle regression.

Gene set enrichment analysis

Gene correlation with time was performed by converting developmental day for each cell to an integer value, with birth at zero, then calculating Spearman rank correlation of normalized gene expression for each gene with time. Gene Set Enrichment Analysis (GSEA) was performed on the correlation coefficients as per the protocol in Reimand et al. (2019), using the quiescence gene set (Cheung and Rando, 2013) and gene sets defined here: http://download.baderlab.org/EM_Genesets/January_01_2020/Mouse/symbol/Mouse_GOBP_AllPathways_no_GO_iea_January_01_2020_symbol.gmt. GSEA calculations were performed in R using the fast GSEA (fgsea) algorithm. Large gene set databases contain redundancy that makes interpretation difficult, so prior to reporting enriched gene sets, the results were collapsed into a non-redundant set (minimizing overlapping genes per set) using a Bayesian network construction approach (Korotkevich et al., 2019).

ICA data analysis

Independent Component Analysis was performed on the combined RP/NSC dataset in R using the FastICA algorithm. The goal was to find two independent components that uniquely represented transcriptional differences between adult dNSCs and embryonic RPs, and cortical versus GE RPs. ICA was performed iteratively with different numbers of components, and in each round components were tested for their ability to maximize these differences in their cell embeddings. ICA with 11 components was selected because components 1 and 11 showed the most difference between cell populations and were unique in their ability to do so – no other components in the mixture separated these populations. Projection of adult NSCs and TAPs into the ICA cell embedding was performed after scaling their transcriptomes using the original data’s scaling factors, by multiplying the cross-product of the new data and whitening matrix with the gene loadings. GSEA calculations on gene loadings for components 1 and 11 were performed

as above, with custom gene sets for glutamatergic (*Neurog1*, *Neurog2*, *Eomes*, *Emx1*, *Emx2*, *Pax6*, *Fezf2*) and GABAergic (*Dlx2*, *Dlx1*, *Gsx2*, *Ascl1*, *Olig2*, *Six3*) specifiers added. Tables describing gene sets positively and negatively correlated with components 1 and 11 along with R code are available upon request.

QUANTIFICATION AND STATISTICAL ANALYSIS

Quantification of gene signature

To perform the cortical RP signature gene score analysis depicted in Figures 1J and 2J, we used a previously defined list of 90 embryonic cortical RP core identity genes (Yuzwa et al., 2017) and computed a gene signature score by taking the average expression of all detected RP core identity genes in each cell. Gene signature scores for each cell were subsequently overlaid on the tSNE plot to display cells with the highest signature scores. The same analysis was carried out in Figures 1K and 2K using a newly defined 23 gene signature that is specific to postnatal V-SVZ NSCs. This NSC signature included the following genes: *Tfap2c*, *Vim*, *Tead2*, *Sfrp1*, *Rcn1*, *Rcn3*, *Nes*, *Veph1*, *Tnc*, *Thbs4*, *Tspan18*, *Meg3*, *Vnn1*, *Cpe*, *Fxyd6*, *Igfbp5*, *Dbi*, *Notum*, *Sparc*, *Fabp7*, *Mdfl*, *Shroom3*, and *Ccdc80*. Cut-offs are provided in the figure legends.

Upregulation of quiescence genes over time

To determine upregulation of genes associated with quiescence over time (Figure 5J), gene correlation with time was performed by converting developmental day for each cell to an integer value, with birth at zero, then calculating Spearman rank correlation of normalized gene expression for each gene with time (same method as was done in the GSEA). Quiescence genes were determined to be more correlated with time by comparing Spearman rank correlation coefficients versus all other detected genes using the Wilcoxon rank-sum test. Significance values are given in the figure legend and results section.

Quantification of ambient RNA contamination fraction

Ambient RNA contamination fractions in single cell RNA-Seq datasets were determined using the SoupX package (version 0.3.1). 4 genes highly expressed in immune cells (*Hexb*, *C1qa*, *C1qb*, and *C1qc*) were manually chosen as “Soup specific genes” to estimate the ambient RNA contamination fraction in each single cell RNA-Seq dataset analyzed. Contamination fractions were subsequently calculated using the `calculateContaminationFraction` function.

Differential gene expression statistical analysis

Statistics used to test differential gene expression in the scRNA-Seq data was performed using the `Seurat FindMarkers` function. An adjusted p value (FWER) smaller than 0.05 was considered statistically significant (Bonferroni-Holm method). Specific significance values are given in supplemental tables. For Table S7, only genes with an average log fold change greater than 0.5 are shown.

Cluster assignment statistical analysis

Single cells were assigned to distinct clusters using SNN-Cliq-inspired clustering (`FindClusters` function in `Seurat`) at increasing resolutions ensuring the number of differentially expressed genes (determined by the `FindMarkers` function in `Seurat`) between most similar clusters was greater or equal to 30 genes. In this analysis, an adjusted p value (FWER) smaller than 0.01 was considered statistically significant (Bonferroni-Holm method).

Pearson correlation analysis

Pearson correlation analysis was carried out by averaging the expression of each gene in a given cluster or cell type and performing Pearson correlation using the `cor.test` function in R. r values are provided in the figure legends and results text. The single cell Pearson correlation analysis depicted in Figures 5I, 6G and 6H was carried out as previously described (Storer et al., 2020). Average transcriptomes were calculated for adult dNSCs, E14 total cortical and GE RPs, E14 cortical RPs, and E14 GE RPs by averaging the expression of each detected gene in each cell type. Each cell depicted on the plot was subsequently correlated to each of the 4 average transcriptomes using Pearson correlation. X-coordinates represent the difference between the correlation of a cell with the adult quiescent dNSC average transcriptome and the correlation of the same cell with the E14 total RP average transcriptome. Y-coordinates represent the difference between the correlation of a cell with the E14 cortical RP average transcriptome and the correlation of the same cell with the E14 GE RP average transcriptome.

GSEA statistical analysis

False discovery rates reported in the GSEA analysis were calculated using the Benjamini-Hochberg method. $FDR \leq 0.01$ was considered to be statistically significant with the exception of GSEA calculations on gene loadings for component 11 in ICA analysis (Figure 7F), in which case an $FDR < 0.1$ was considered to be statistically significant. Specific significance values are provided in the supplemental tables.

Morphological analysis

All morphological analyses were performed on at least 3 different brains each.

Additional details of the statistical analyses and software can be found in the detailed descriptions of the computational methods above and, where relevant, in the results and the figure legends. For all morphological analyses, n refers to number of animals analyzed, while for the scRNA-seq analyses, n refers to independent sequencing runs that each included tissue from multiple mice. For the E14 Emx1Cre scRNA-seq runs, $n = 2$ and $n = 3$ consisted of independent scRNA-sequencing runs from the same litter of mice. In all other cases, scRNA-Seq replicates were each performed on different mouse litters. No additional methods were used to determine whether the data met assumptions of the statistical approaches used.